nature portfolio

https://doi.org/10.1038/s41586-025-09052-5

Supplementary information

Increased CSF drainage by non-invasive manipulation of cervical lymphatics

In the format provided by the authors and unedited

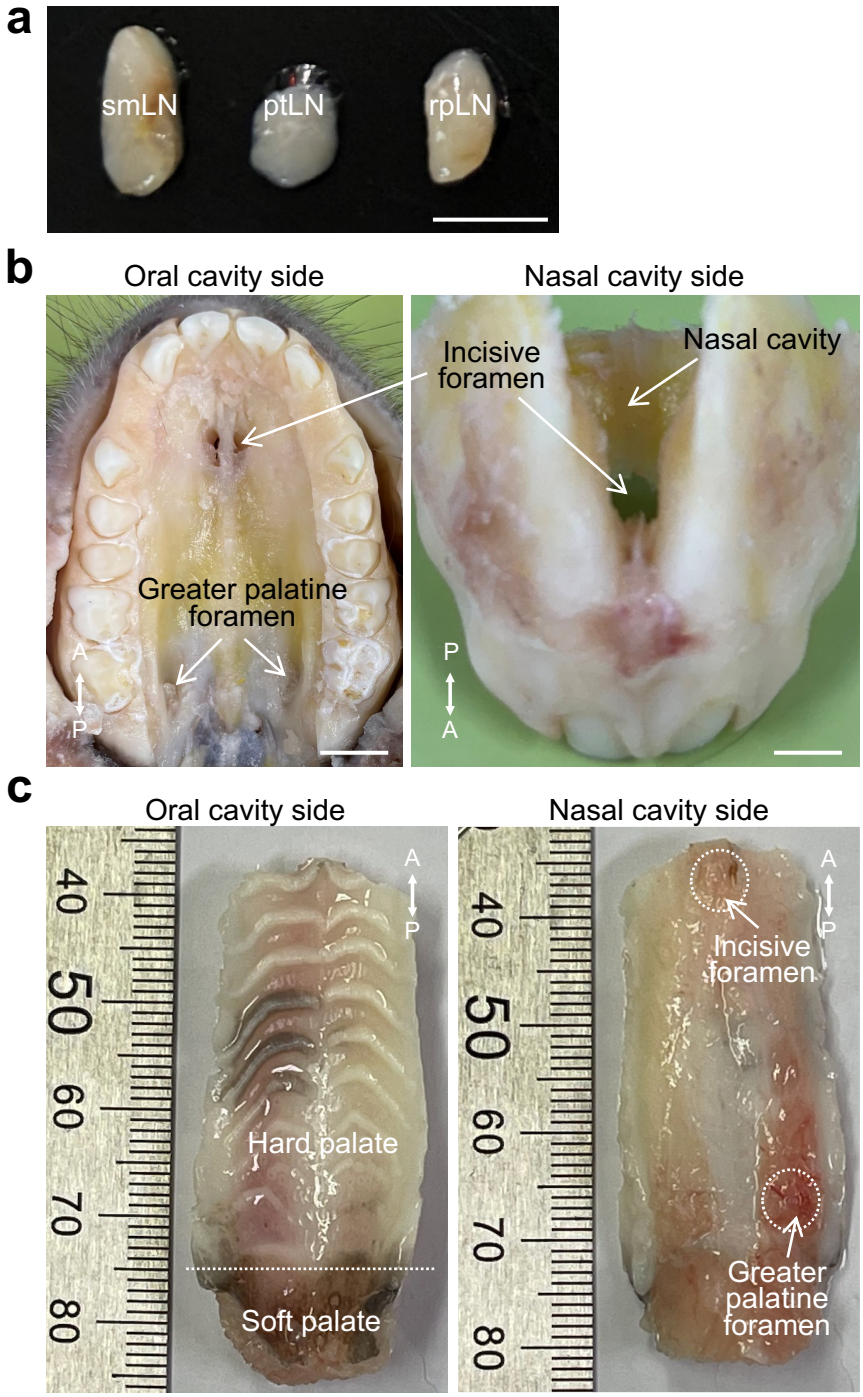

Supplementary Fig. 1. Structural features of cervical lymph nodes and hard palate of *Macaca fascicularis* monkeys

a, Brightfield microscopic image of the submandibular lymph node (smLN), parotid lymph node (ptLN), and retropharyngeal lymph node (rpLN). Scale bar, 5 mm.

b, Brightfield image of the roof of the mouth (left) showing the greater palatine foramen and incisive foramen in a *Macaca fascicularis* monkey. View from the nasal cavity (right) showing the connection to the oral cavity through the incisive foramen. Scale bars, 5 mm. Representative of *n* = 2 monkeys from two independent experiments.

c, Brightfield images of the oral (left) and nasal (right) surfaces of the hard palate of a *Macaca fascicularis* monkey. White dashed line (left) marks the approximate boundary between the hard palate and soft palate. White dashed circles (right) mark the location of the incisive foramen and greater palatine foramen in the hard palate. Representative of *n* = 2 monkeys from two independent experiments.

Anatomical positions are indicated in the bottom left (**b**) or upper right (**c**) corner: A, anterior; P, posterior.

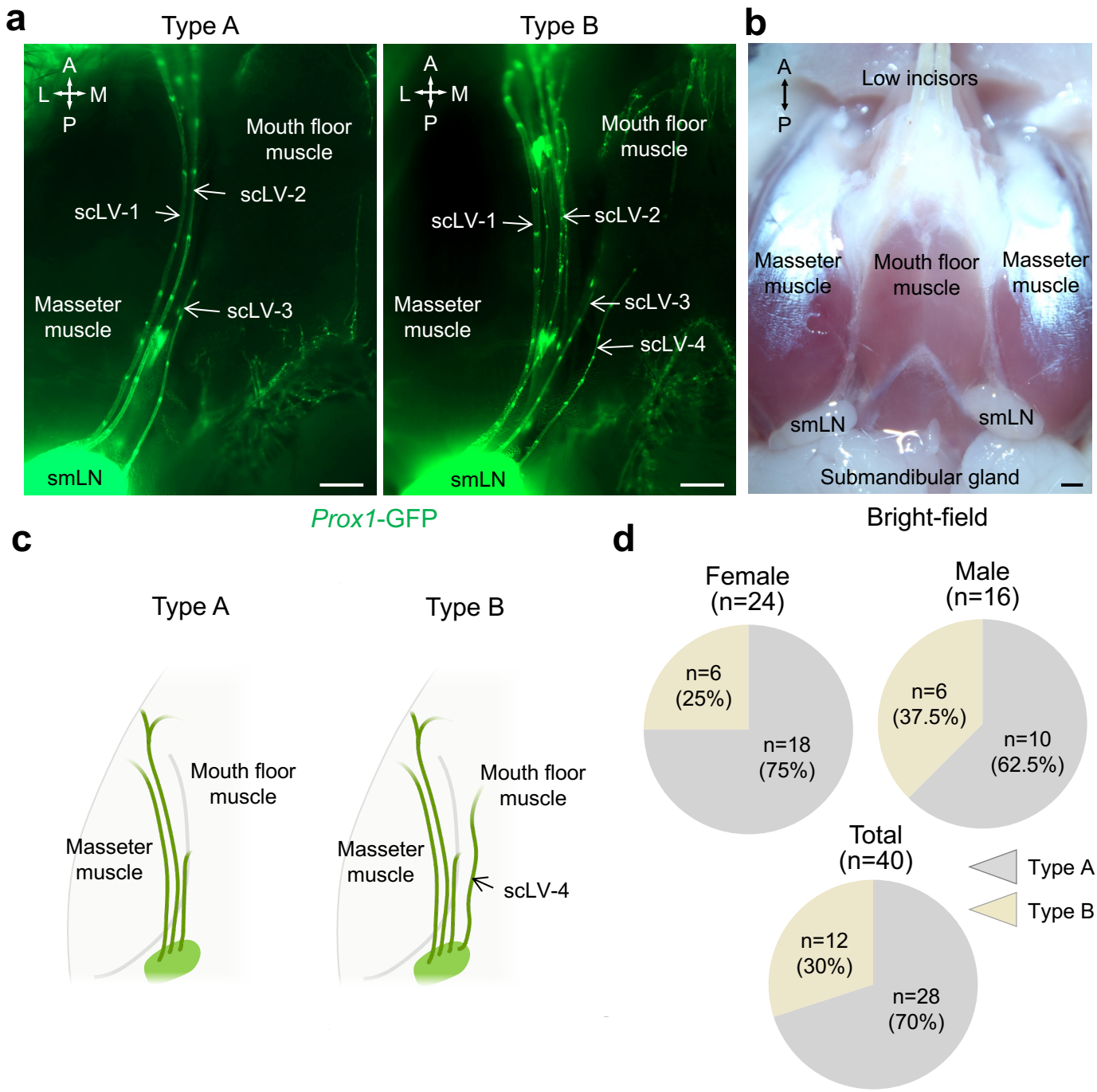

Supplementary Fig. 2. Three or four superficial cervical lymphatics join the submandibular lymph node in mice

a-c, Fluorescence and brightfield microscopic images (representative images from five independent experiments) (**a,b**) and drawings (**c**) that compare *Prox1*-GFP mice with three (Type A: scLV-1, scLV-2, scLV-3) or four (Type B: scLV-1, scLV-2, scLV-3, scLV-4) superficial cervical lymphatics that join the submandibular lymph node (smLN). The structures are located superficial to and between the masseter and mouth floor muscles. Anatomical positions are indicated in the top left corner: A, anterior; P, posterior; M, medial; L, lateral. Scale bars, 1 mm.

d, Pie charts showing the percentage of Type A mice (gray) with three superficial cervical lymphatics and Type B mice (beige) with four superficial cervical lymphatics that join the submandibular lymph node in female (*n* = 24), male (*n* = 16), and all (*n* = 40) mice.

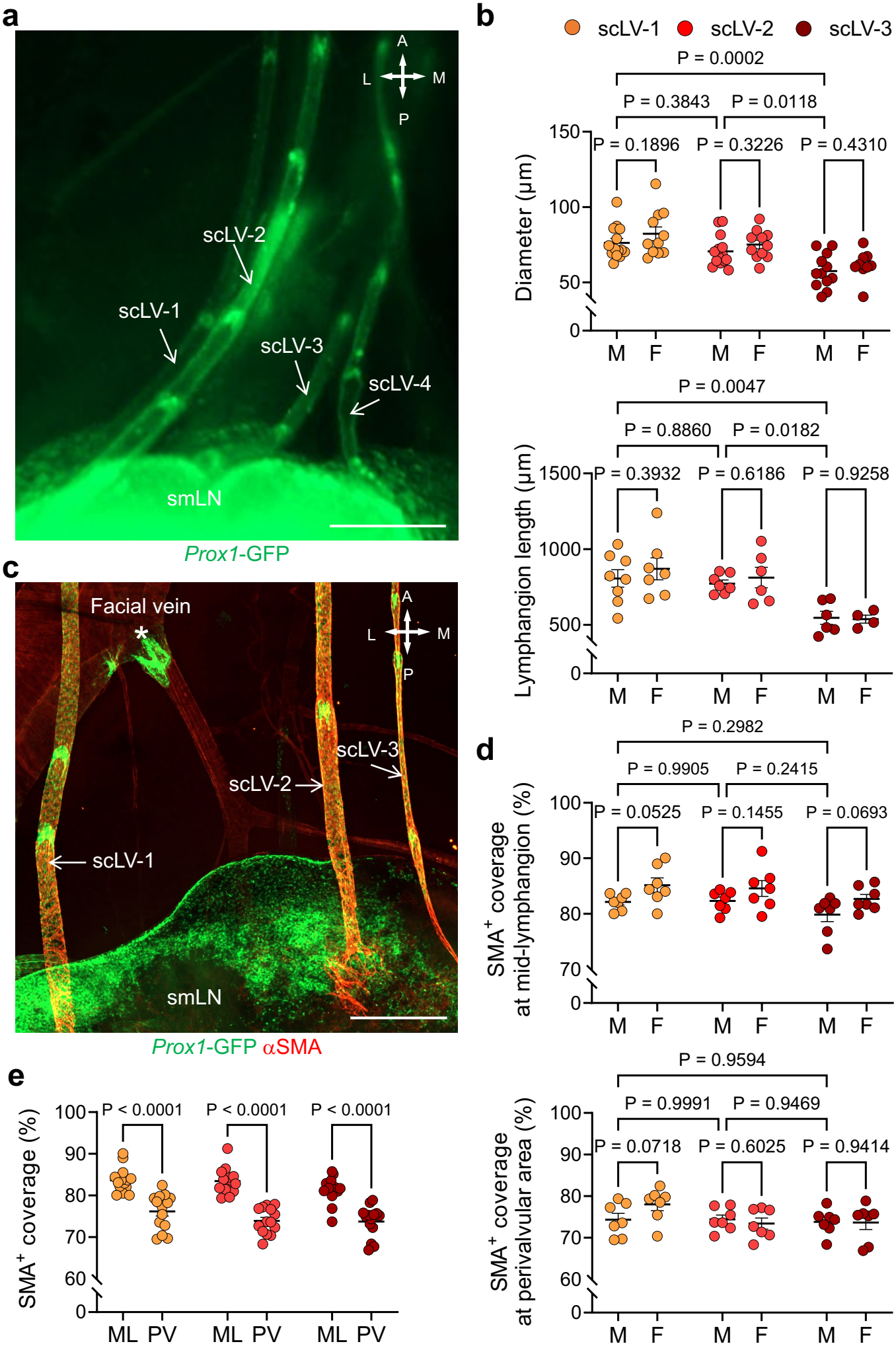
a
A
L
M
P
scLV-2
scLV-1
scLV-3
scLV-4
smLN
Prox1-GFP
b
scLV-1
scLV-2
scLV-3
P = 0.0002
P = 0.3843
P = 0.0118
P = 0.1896
P = 0.3226
P = 0.4310
Diameter (μm)
150
100
50
0
M F M F M F
P = 0.0047
P = 0.8860
P = 0.0182
P = 0.3932
P = 0.6186
P = 0.9258
Lymphangion length (μm)
1500
1000
500
0
M F M F M F
c
Facial vein
*
A
L
M
P
scLV-3
scLV-2
scLV-1
smLN
Prox1-GFP αSMA
d
P = 0.2982
P = 0.9905
P = 0.2415
P = 0.0525
P = 0.1455
P = 0.0693
SMA+ coverage at mid-lymphangion (%)
100
90
80
70
0
M F M F M F
P = 0.9594
P = 0.9991
P = 0.9469
P = 0.0718
P = 0.6025
P = 0.9414
SMA+ coverage at perivalvular area (%)
100
90
80
70
60
0
M F M F M F
e
P < 0.0001
P < 0.0001
P < 0.0001
SMA+ coverage (%)
100
90
80
70
60
0
ML PV ML PV ML PV

Supplementary Fig. 3. Diameter and length of superficial cervical lymphatics that join the submandibular lymph node

a, Fluorescence image of mouse with four superficial cervical lymphatics (scLV-1, scLV-2, scLV-3, scLV-4) that join the submandibular lymph node (smLN) of a *Prox1*-GFP mouse. The view is similar to images in **Supplementary Fig. 2a.** Scale bar, 500 μm. Representative of *n* = 25 mice from four independent experiments.

b, Comparison of the diameter and length of lymphangions (lymphatic segment between the valves) of scLV-1, scLV-2, and scLV-3 in male (M) and female (F) *Prox1*-GFP mice. Diameters were similarly variable in scLV-1 (62-115 μm) and scLV-2 (58-92 μm) but were larger than those of scLV-3 (40-76 μm). Lymphangion lengths were also similarly variable in scLV-1 (543-1,238 μm) and scLV-2 (638-1,052 μm) but were longer than those of scLV-3 (423-673 μm). No significant sex differences were found. Each dot is the value for one mouse. *n* = 14 (scLV-1 and scLV-2) or 12 (scLV-3) male mice (diameter), *n* = 11 (scLV-1 and scLV-2) or 9 (scLV-3) female mice (diameter), *n* = 8 (scLV-1) or 7 (scLV-2) or 6 (scLV-3) male mice (length), *n* = 7 (scLV-1) or 6 (scLV-2) or 4 (scLV-3) female mice (length) per group from four independent experiments. Error bars indicate mean ± s.e.m. *P* values calculated by two-way ANOVA followed by two-tailed Tukey's multiple-comparison post hoc test.

c, Immunofluorescence image of whole mounts showing superficial cervical lymphatics scLV-1, scLV-2, and scLV-3 that join the submandibular lymph node (smLN) of a *Prox1*-GFP mouse. The white asterisk marks a *Prox1*-GFP$^+$ valve of the facial vein. Scale bar, 500 μm. Representative of *n* = 14 mice in four independent experiments.

d,e, Comparison of the percent smooth muscle coverage of perivalvular (PV, upper graph) and mid-lymphangion (ML, lower graph) regions of scLV-1, scLV-2, and scLV-3 in male (M) and female (F) *Prox1*-GFP mice (**d**). Percent overall smooth muscle coverage of the lymphatics is also shown (**e**). Each dot is the value for one mouse. *n* = 7 (male), *n* = 7 (female) mice per group from four independent experiments. All measurements were made in the same mice. Error bars indicate mean ± s.e.m. *P* values calculated by two-way ANOVA followed by two-tailed Tukey's or Sidak's multiple-comparison post hoc test .

Anatomical positions are indicated in the top right corner: A, anterior; P, posterior; M, medial; L, lateral.

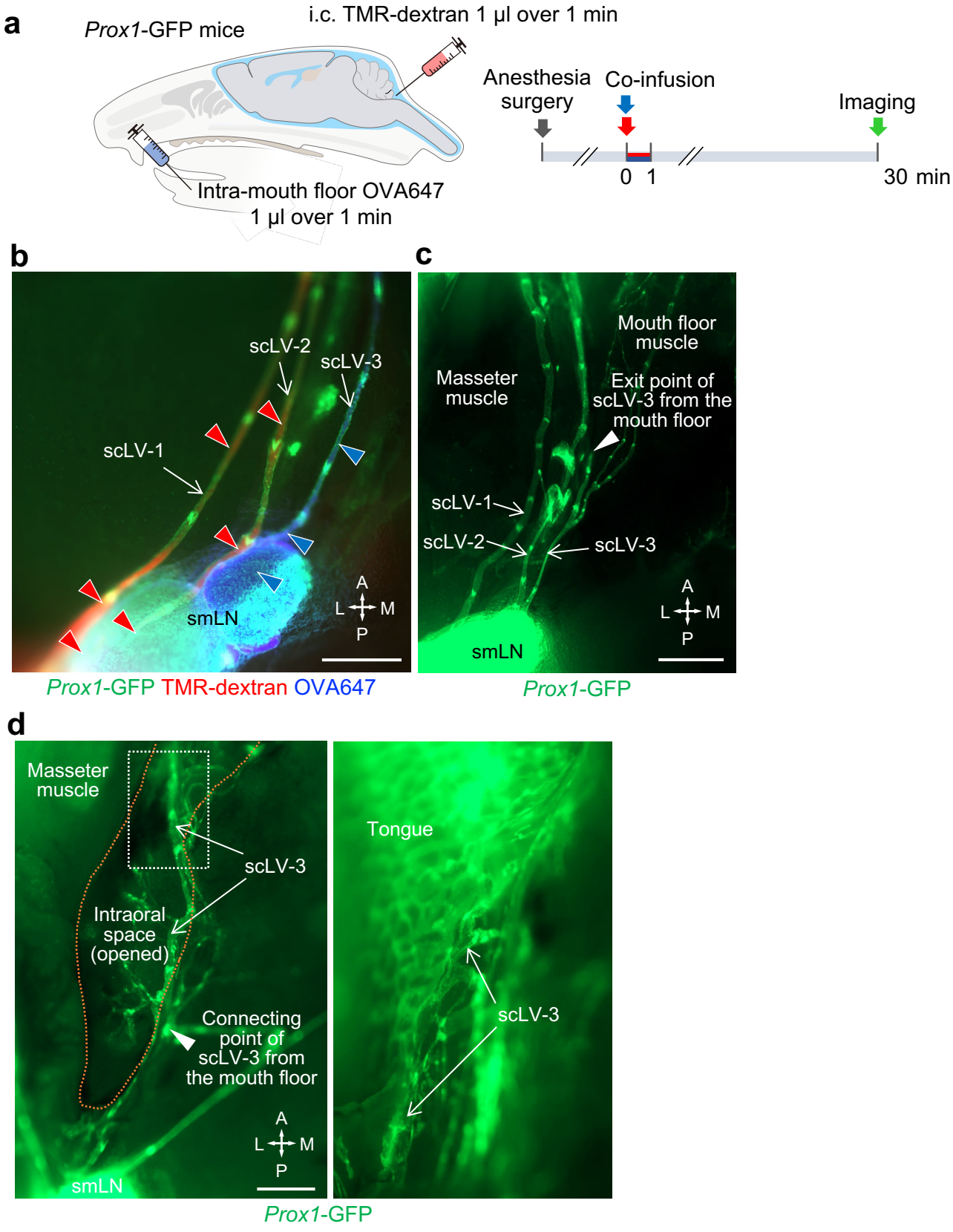
a
Prox1-GFP mice
i.c. TMR-dextran 1 µl over 1 min
Intra-mouth floor OVA647
1 µl over 1 min
Anesthesia surgery
Co-infusion
Imaging
0 1
30 min
b
scLV-2
scLV-3
scLV-1
smLN
A
L
M
P
Prox1-GFP TMR-dextran OVA647
c
Mouth floor muscle
Masseter muscle
Exit point of scLV-3 from the mouth floor
scLV-1
scLV-2
scLV-3
smLN
A
L
M
P
Prox1-GFP
d
Masseter muscle
scLV-3
Intraoral space (opened)
Connecting point of scLV-3 from the mouth floor
smLN
A
L
M
P
Tongue
scLV-3
Prox1-GFP

Supplementary Fig. 4. Submandibular lymph node receives CSF drainage and facial lymph through separate superficial cervical lymphatics

a, Sequence of simultaneous intracisternal (i.c.) infusion of 1.0 µl TMR-dextran and injection of 1.0 µl Alexa-647-conjugated ovalbumin (OVA647) into the mouth floor of *Prox1*-GFP mice over 1 min followed by imaging of both fluorescent tracers in superficial cervical lymphatics and submandibular lymph node (smLN) 30 min later.

b, Fluorescence image showing TMR-dextran fluorescence (red arrowheads) that is strong in superficial cervical lymphatic scLV-1, moderate in scLV-2, and absent in scLV-3 where they join the submandibular lymph node (smLN). However, OVA647 fluorescence is absent in scLV-1 and scLV-2 but strong in scLV-3 and in the submandibular lymph node (blue arrowheads). Scale bar, 1 mm. Representative of $n = 4$ mice from three independent experiments.

c, Fluorescence image of the cervical region of a *Prox1*-GFP mouse showing the short course of superficial cervical lymphatic scLV-3 from the mouth floor (white arrowhead) to the submandibular lymph node (smLN) next to the longer course of scLV-1 and scLV-2 that extends outside the image. White arrowhead marks the exit point of scLV-3 from the mouth floor. Scale bar, 1 mm. Representative of $n = 4$ mice from three independent experiments.

d, Fluorescence images of superficial cervical lymphatic scLV-3 near the masseter muscle viewed from the open mouth of a *Prox1*-GFP mouse showing connections with mouth floor lymphatics and the submandibular lymph node (smLN). Orange dashed line marks the boundary of the mouth and cervical regions. White dashed line box (left) marks the region enlarged in the other image (right). White arrowhead (left) indicates the exit point of scLV-3 from the mouth floor. Scale bar, 1 mm. Representative of $n = 4$ mice from three independent experiments.

Anatomical positions are indicated in the bottom right corner: A, anterior; P, posterior; M, medial; L, lateral.

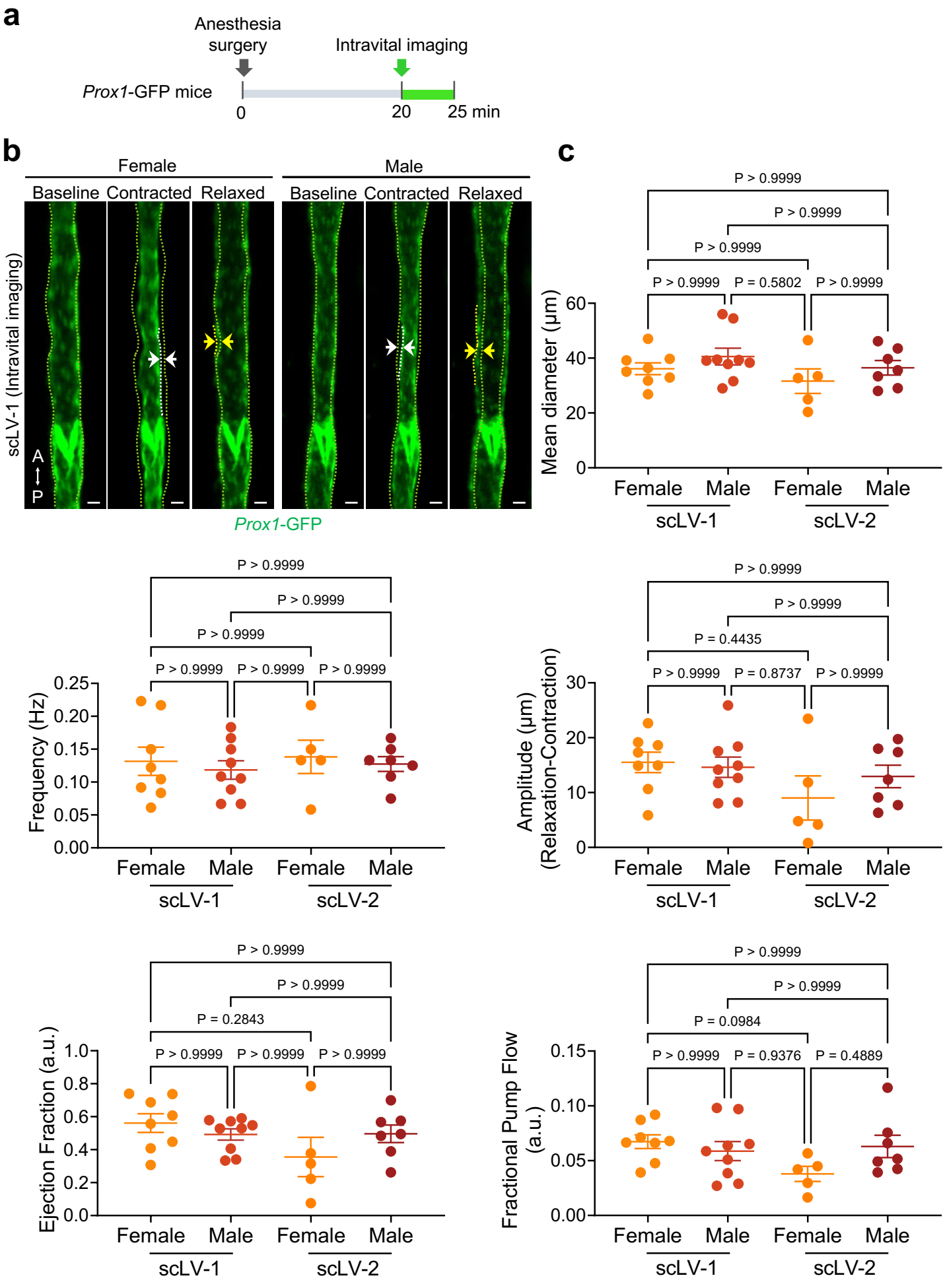
a
Anesthesia surgery
Intravital imaging
Prox1-GFP mice
0
20
25 min
b
Female
Male
Baseline
Contracted
Relaxed
Baseline
Contracted
Relaxed
scLV-1 (Intravital imaging)
A
P
Prox1-GFP
c
Mean diameter (μm)
P > 0.9999
P > 0.9999
P > 0.9999
P > 0.9999
P = 0.5802
P > 0.9999
0
20
40
60
Female
Male
Female
Male
scLV-1
scLV-2
Frequency (Hz)
P > 0.9999
P > 0.9999
P > 0.9999
P > 0.9999
P > 0.9999
P > 0.9999
0.00
0.05
0.10
0.15
0.20
0.25
Female
Male
Female
Male
scLV-1
scLV-2
Amplitude (μm) (Relaxation-Contraction)
P > 0.9999
P > 0.9999
P = 0.4435
P > 0.9999
P = 0.8737
P > 0.9999
0
10
20
30
Female
Male
Female
Male
scLV-1
scLV-2
Ejection Fraction (a.u.)
P > 0.9999
P > 0.9999
P = 0.2843
P > 0.9999
P > 0.9999
P > 0.9999
0.0
0.2
0.4
0.6
0.8
1.0
Female
Male
Female
Male
scLV-1
scLV-2
Fractional Pump Flow (a.u.)
P > 0.9999
P > 0.9999
P = 0.0984
P > 0.9999
P = 0.9376
P = 0.4889
0.00
0.05
0.10
0.15
Female
Male
Female
Male
scLV-1
scLV-2

Supplementary Fig. 5. Similarity of physiologic properties of superficial cervical lymphatics scLV-1 and scLV2 in both sexes

a, Sequence of intravital imaging of superficial cervical lymphatics scLV-1 and scLV-2 of *Prox1*-GFP mice. Intravital imaging over 5 min began after a 20 min stabilization period.

b, Intravital images of spontaneously contracted and relaxed scLV-1 in female and male *Prox1*-GFP mice. The baseline images were captured at the middle of contraction and relaxation. Green dashed line outlines the size at baseline. Arrows indicate the maximum diameter difference from the baseline during contraction (white arrow) and relaxation (yellow arrow). Anatomical positions are indicated in the bottom left corner: A, anterior; P, posterior. Scale bars, 20 μm. Representative of *n* = 5-9 mice from three independent experiments.

c, Dot plots showing no significant differences in mean diameter, frequency, amplitude, ejection fraction, and fractional pump flow of superficial cervical lymphatics scLV-1 and scLV-2 of male and female *Prox1*-GFP mice. Each dot is the value for one mouse. *n* = 8 (scLV-1, female) or 9 (scLV-1, male) or 5 (scLV-2, female) or 7 (scLV-2, male) mice of each sex in three independent experiments. Error bars indicate mean ± s.e.m. a.u., arbitrary unit. *P* values calculated by Kruskal-Wallis test followed by two-tailed Dunn's multiple comparison post hoc test.

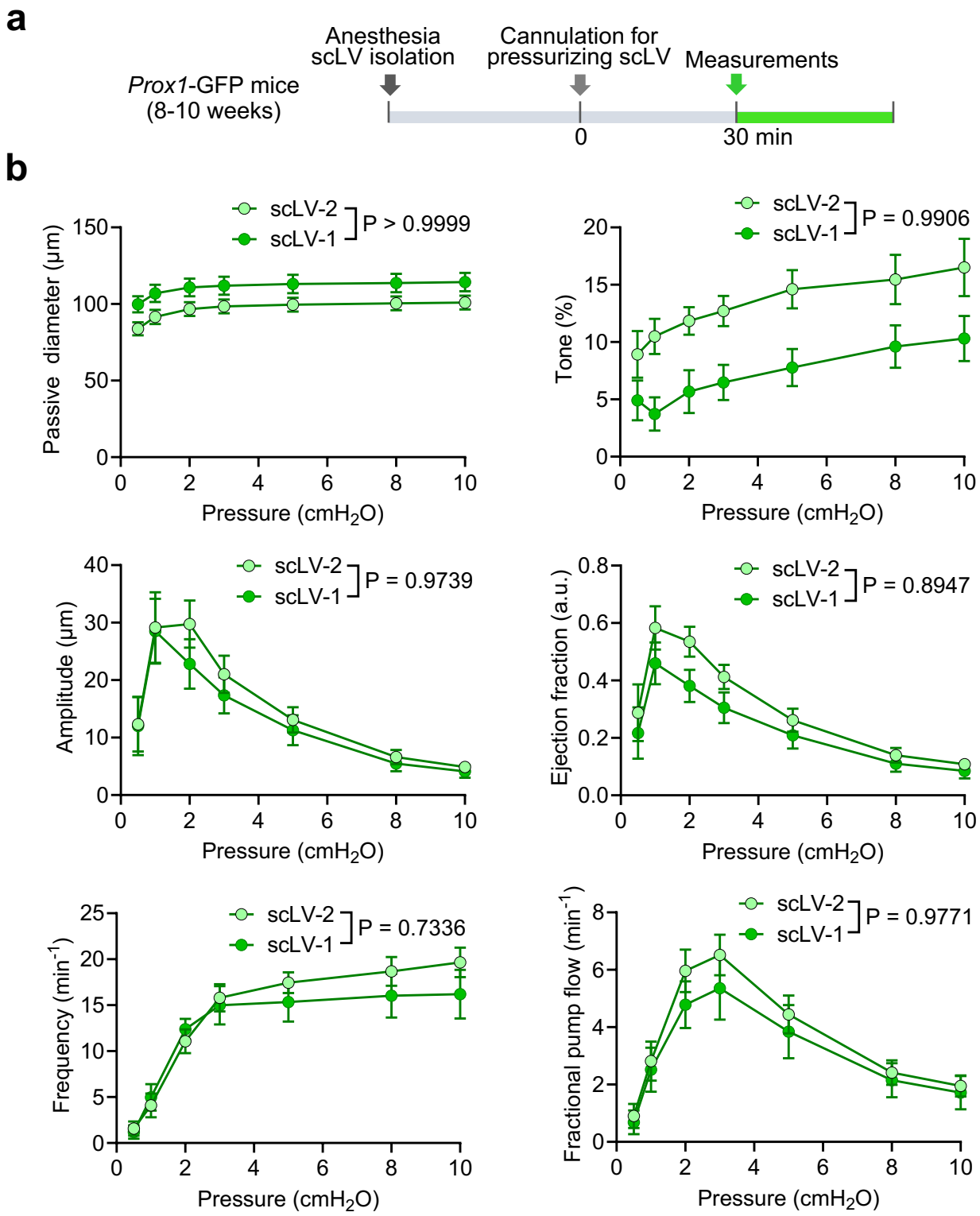

Supplementary Fig. 6. Responses of isolated superficial cervical lymphatics to pressure changes

a, Sequence of isolation and measurement of responses of superficial cervical lymphatics scLV-1 and scLV-2 from adult *Prox1*-GFP (8-10 weeks) mice to pressure changes within the physiological range of 0.5 to 10 cmH_2O.

b, Line plots showing no significant differences in passive diameter, tone, amplitude, ejection fraction, frequency, and fractional pump flow between scLV-1 and scLV-2 over pressures ranging from 0.5 to 10 cmH_2O. Each dot is the value for one mouse. n = 10 mice of both sexes from three independent experiments. Error bars indicate mean ± s.e.m. P values calculated by two-way ANOVA test followed by two-tailed Sidak's multiple comparison test. P values represent the significance of the interaction between pressure and scLV-1 or scLV-2.

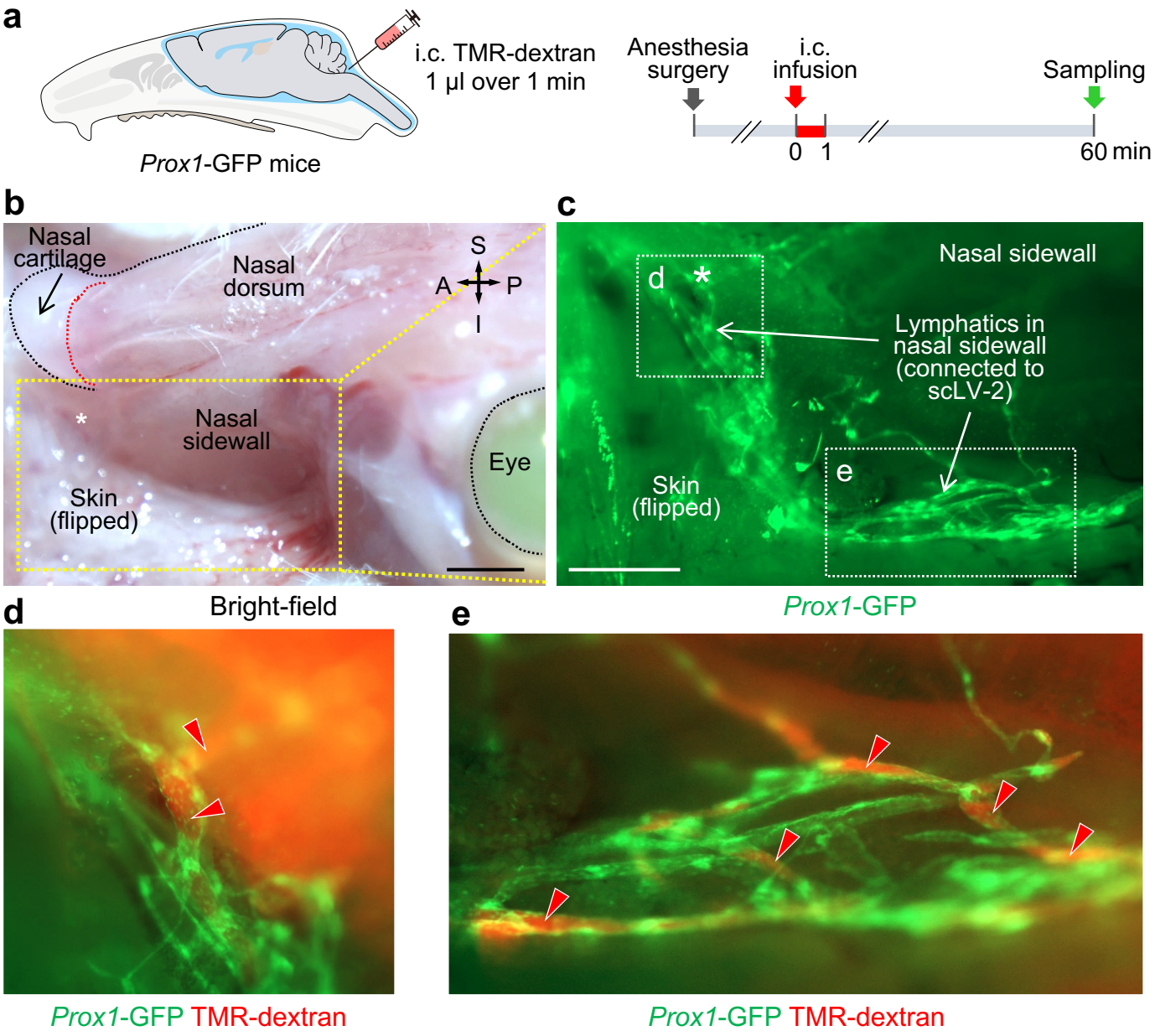

Supplementary Fig. 7. CSF drainage through lymphatics in the nasal mucosa en route to the nasal sidewall

a, Sequence of intracisternal (i.c.) infusion of 1.0 µl TMR-dextran over 1 min into *Prox1*-GFP mice followed by imaging of TMR-dextran in lymphatics in the nasal sidewall 60 min later.

b, Brightfield microscopic image showing location of the nasal side wall. Red dashed line marks the nasal bone-cartilage junction. Black dashed lines marks the contour of the nose and eye. Region marked by yellow dashed line box is enlarged in fluorescence microscopic image in (**c**). Anatomical positions are indicated in the top right corner: S, superior; I, inferior; A, anterior; P, posterior. Scale bars, 1mm. Representative of *n* = 4 mice from three independent experiments.

c-e, Fluorescence microscopic images showing nasal sidewall lymphatics (green) (**c**) and TMR-dextran (red) within these lymphatics (**d,e**). White asterisk in (**c**) marks the connection between lymphatics in the nasal mucosa and nasal sidewall. White dashed line boxes in (**c**) are enlarged in (**d**) and (**e**). TMR-dextran containing lymphatics in the nasal sidewall in (**d,e**) are connected to superficial cervical lymphatic scLV-2 (red arrowheads). Scale bars, 1mm. Representative of *n* = 4 mice from three independent experiments.

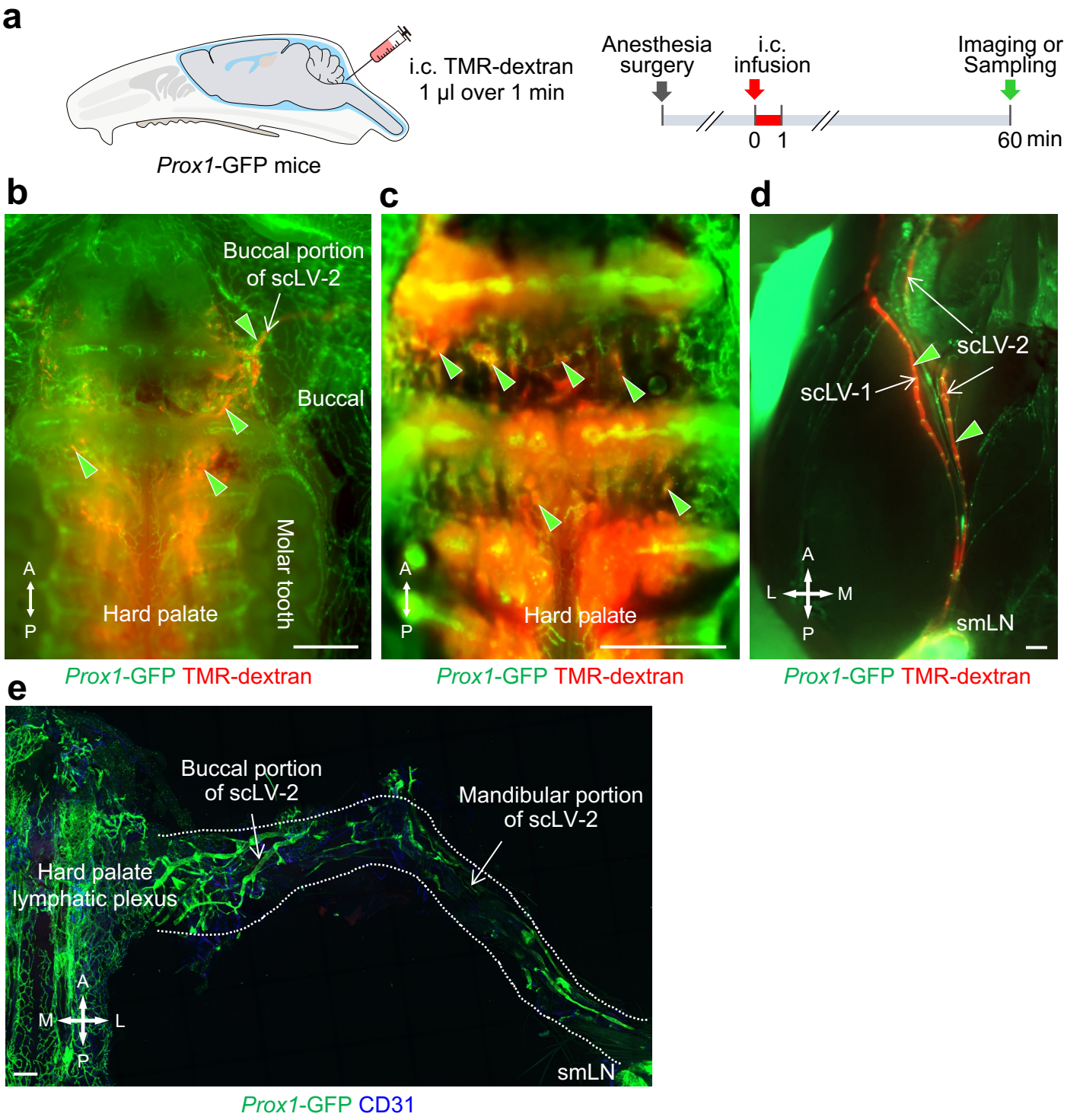

Supplementary Fig. 8. Connection of hard palate lymphatic plexus to superficial cervical lymphatics

a, Sequence of intracisternal (i.c.) infusion of 1.0 µl TMR-dextran over 1 min into *Prox1*-GFP mice followed by imaging of TMR-dextran in lymphatics of the hard palate plexus and their downstream connections 60 min later.

b-e, Fluorescence microscopic images of whole mounts showing the hard palate lymphatic plexus and downstream connections to superficial cervical lymphatics in *Prox1*-GFP mice. TMR-dextran is shown in hard palate lymphatic plexus and scLV-1 and scLV-2 (green arrowheads, **b-d**). White dashed lines mark the lymphatic pathway (green) from the hard palate lymphatic plexus through buccal and mandibular portions of scLV-2 to the submandibular lymph node (smLN) (**e**). Anatomical positions are indicated in the bottom left corner: A, anterior; P, posterior; M, medial; L, lateral. Scale bars, 1 mm. Representative of *n* = 15 mice from nine independent experiments.

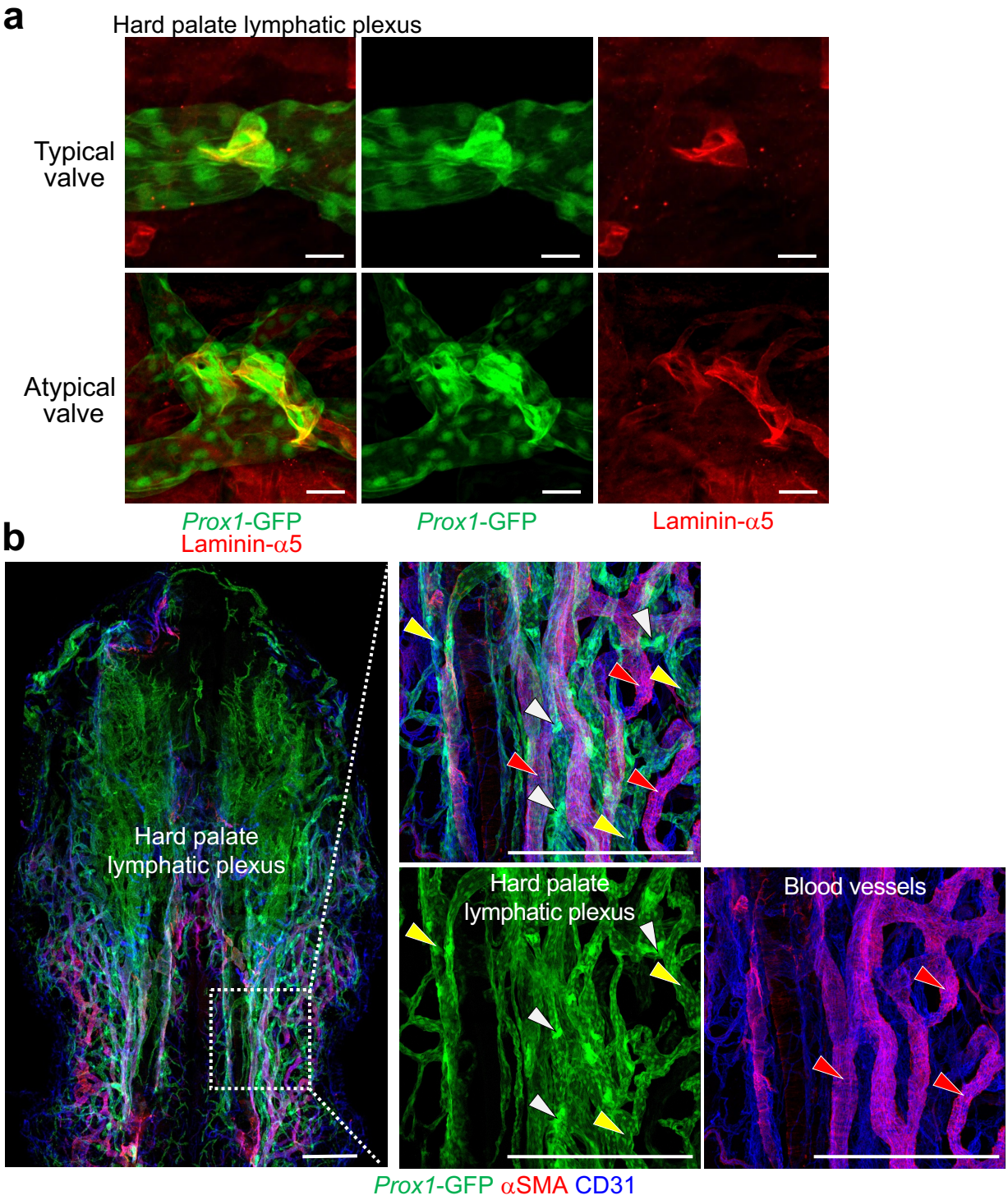

Supplementary Fig. 9. Hard palate lymphatics have heterogeneous valves but no smooth muscle coverage

a, Immunofluorescence images of a whole mount showing two types of lymphatic valves in lymphatics of the hard palate lymphatic plexus of *Prox1*-GFP mice. Typical bicuspid valves are semilunar in shape (upper row), whereas atypical valves have an irregular or linear shape (lower row). Both types of valves have strong Prox1 (green) and laminin-α5 (red) immunoreactivities. Scale bars, 20 μm. Representative of *n* = 3 mice from three independent experiments.

b, Immunofluorescence images of a whole mount of the hard palate lymphatic plexus in a *Prox1*-GFP mouse comparing abundant smooth muscle cells (α-smooth muscle actin, αSMA staining, red arrowheads) on blood vessels to no smooth muscle cells around mid-lymphangion or perivalvular regions of lymphatics (*Prox1*-GFP, yellow arrowheads). Valves in lymphatics are conspicuous because the bright green *Prox1*-GFP (white arrowheads). White dashed line boxed region in left image is enlarged in the middle and right panels. Scale bars, 500 μm. Representative of *n* = 3 mice from three independent experiments.

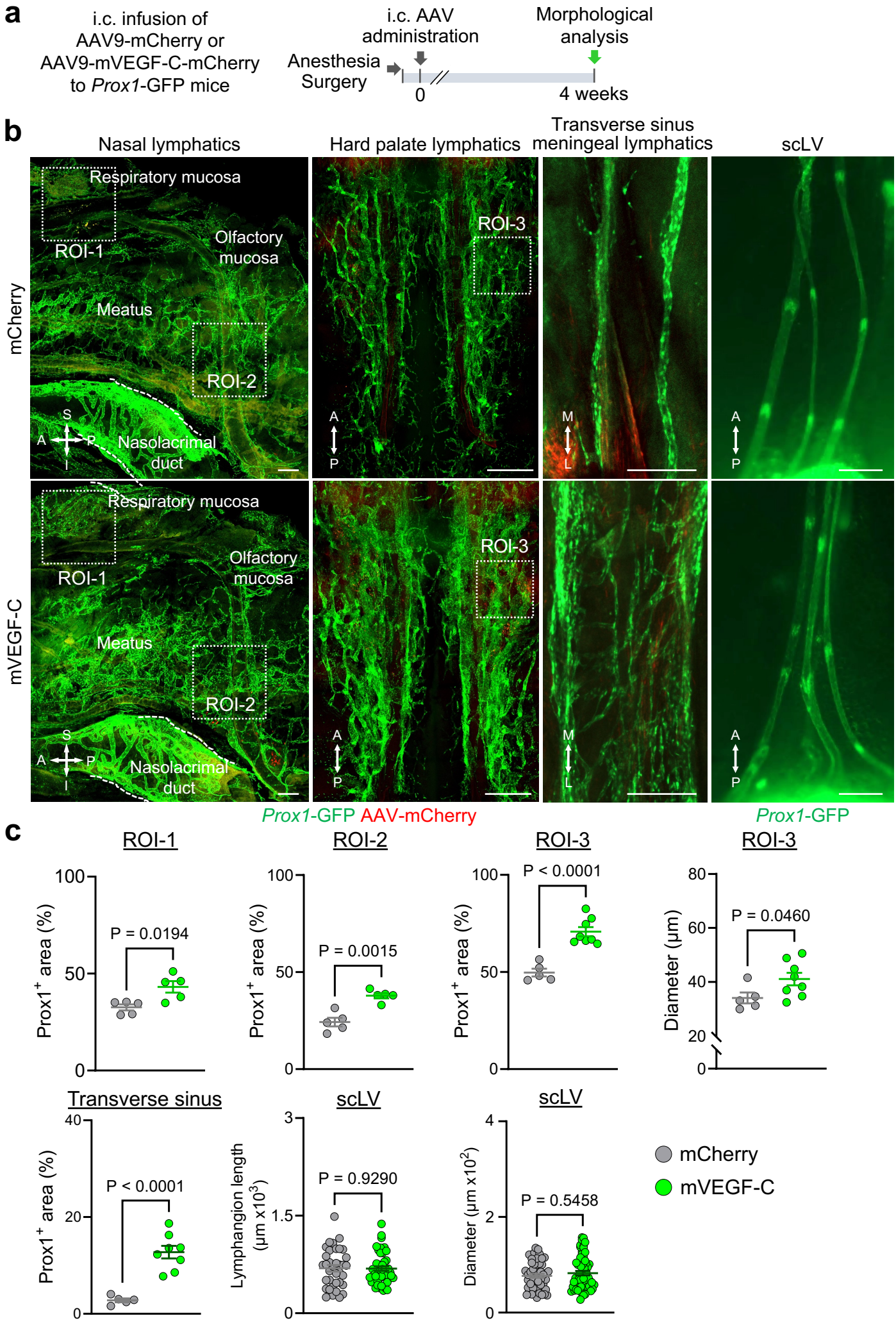
a
i.c. infusion of AAV9-mCherry or AAV9-mVEGF-C-mCherry to Prox1-GFP mice
i.c. AAV administration
Anesthesia Surgery
0
Morphological analysis
4 weeks
b
Nasal lymphatics
Hard palate lymphatics
Transverse sinus meningeal lymphatics
scLV
mCherry
mVEGF-C
Respiratory mucosa
Olfactory mucosa
Meatus
Nasolacrimal duct
ROI-1
ROI-2
ROI-3
Prox1-GFP AAV-mCherry
Prox1-GFP
c
ROI-1
ROI-2
ROI-3
ROI-3
Prox1+ area (%)
P = 0.0194
P = 0.0015
P < 0.0001
Diameter (μm)
P = 0.0460
Transverse sinus
scLV
scLV
Prox1+ area (%)
P < 0.0001
Lymphangion length (μm x10^3)
P = 0.9290
Diameter (μm x10^2)
P = 0.5458
mCherry
mVEGF-C

Supplementary Fig. 10. Expansion of nasal and hard palatal lymphatics after intracisternal delivery of AAV-mVEGF-C

a, Sequence of intracisternal (i.c.) infusion of 1 x 10^{13} genome copies of AAV9-mCherry (mCherry) or AAV9-mVEGF-C-mCherry (mVEGF-C) in 1 µl of PBS over 1 min into adult *Prox1*-GFP mice, followed 4 weeks later by removal of meninges, nasal mucosa, hard palate, and superficial cervical lymphatics (scLV) for immunofluorescence analysis.

b, Confocal microscopic images of whole mounts showing lymphatics (green) in the nasal mucosa, hard palate, and dura along the transverse sinus and a segment of the scLV from *Prox1*-GFP mice 4 weeks after infection with adeno-associated virus encoding mCherry or mVEGF-C. mCherry expression (red) is visible in scattered regions of the nasal cavity, hard plate, and meninges. Lymphatics were measured within marked regions of interest (ROI) outlined by white boxes in the respiratory mucosa (ROI-1) and inferior nasal mucosa (ROI-2), and hard palate submucosa near the incisive foramen (ROI-3). The smaller diameter and different anatomical distribution of *Prox1*-GFP$^+$ nasal lymphatics made them readily distinguishable from *Prox1*-GFP$^+$ venous sinusoids [50]. Scale bars; 200 µm (nasal lymphatics), 500 µm (hard palate lymphatics), 200 µm (transverse sinus), and 200 µm (scLV). Representative of *n* = 5 mice (mCherry) and *n* = 5-8 (mVEGF-C) mice from three independent experiments.

c, Measurements of *Prox1*-GFP nasal area and lymphatic diameter to compare the extent and size of lymphatics in regions marked in **b** as ROI-1 (upper nasal mucosa), ROI-2 (inferior nasal mucosa), and ROI-3 (hard palate) of adult *Prox1*-GFP mice after infection with mCherry (*n* = 5) or mVEGF-C adeno-associated virus (*n* = 5 for ROI-1 or ROI-2, *n* = 8 for ROI-3, transverse sinus or scLV). A similar region was measured in the transverse sinus. Each dot is the value for one mouse except for scLV, where multiple lymphangion measurements were made in each mouse (*n* = 5 mice for mCherry or *n* = 8 mice for mVEGF-C). Error bars indicate mean ± s.e.m. *P* values calculated by two-tailed Welch's t test or two-tailed Mann-Whitney *U*-test.

Anatomical positions are indicated in the bottom left corner: S, superior; I, inferior; A, anterior; P, posterior; M, medial; L, lateral.

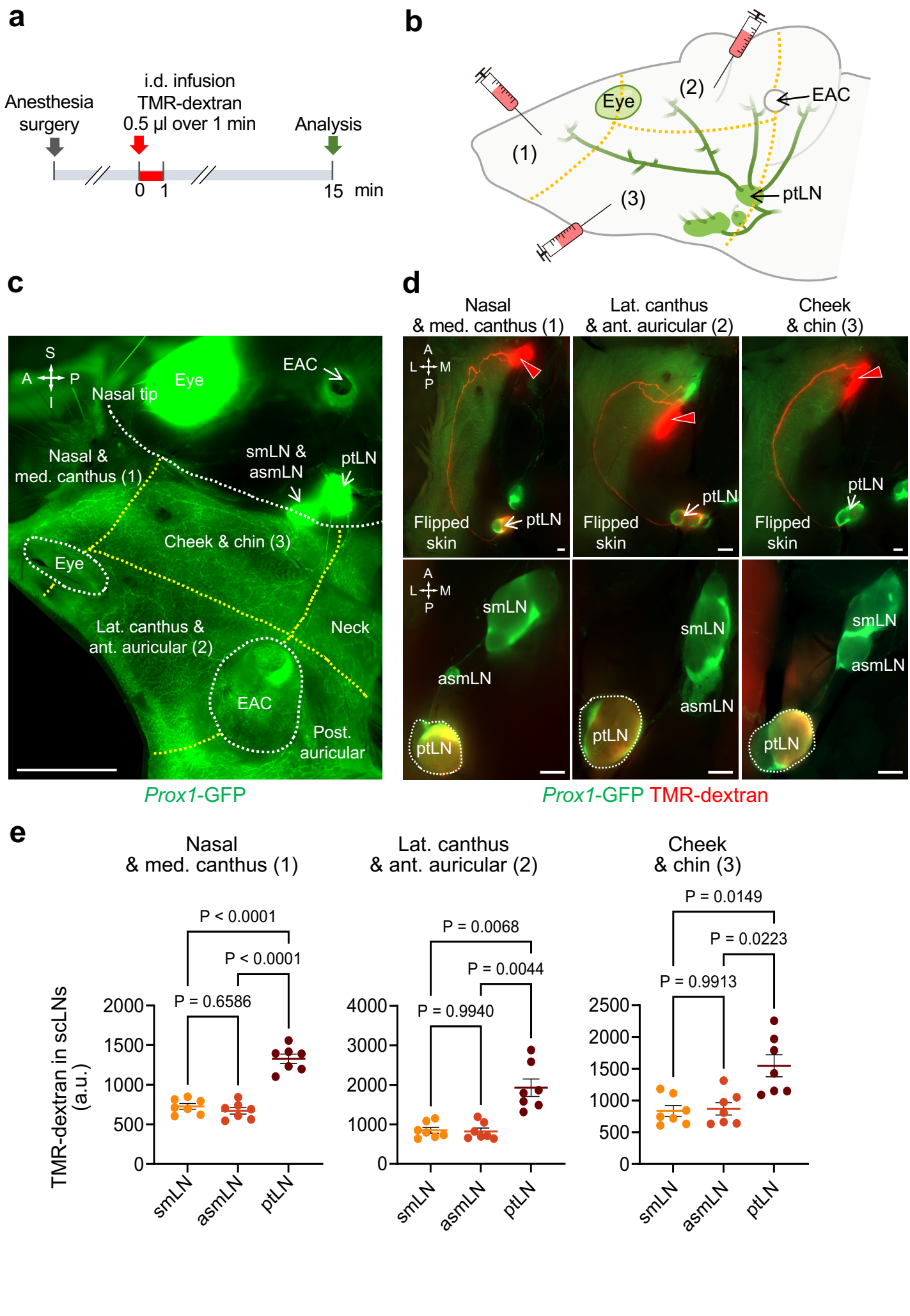
a
Anesthesia surgery
i.d. infusion TMR-dextran 0.5 µl over 1 min
Analysis
0
1
15 min
b
Eye
(2)
EAC
(1)
(3)
ptLN
c
S
A
P
I
Eye
EAC
Nasal tip
Nasal & med. canthus (1)
smLN & asmLN
ptLN
Cheek & chin (3)
Eye
Lat. canthus & ant. auricular (2)
Neck
EAC
Post. auricular
Prox1-GFP
d
Nasal & med. canthus (1)
Lat. canthus & ant. auricular (2)
Cheek & chin (3)
A
L
M
P
Flipped skin
ptLN
smLN
asmLN
Prox1-GFP TMR-dextran
e
Nasal & med. canthus (1)
Lat. canthus & ant. auricular (2)
Cheek & chin (3)
TMR-dextran in scLNs (a.u.)
P < 0.0001
P < 0.0001
P = 0.6586
P = 0.0068
P = 0.0044
P = 0.9940
P = 0.0149
P = 0.0223
P = 0.9913
2000
1500
1000
500
0
4000
3000
2000
1000
0
2500
2000
1500
1000
500
0
smLN
asmLN
ptLN

Supplementary Fig. 11. Facial skin lymph drainage only to parotid lymph node

a, Sequence of intradermal (i.d.) infusion of 0.5 µl TMR-dextran over 1 min into each of three regions of facial skin of *Prox1*-GFP mice followed by imaging of TMR-dextran at the injection site and in superficial cervical lymphatics and lymph nodes 15 min later.

b, Diagram showing the sites of TMR-dextran infusion into facial skin: (1) nasal & medial canthus region; (2) lateral canthus & anterior auricular region; and (3) cheek and chin region. External auditory canal (EAC). Parotid lymph node (ptLN).

c, Fluorescence image of facial skin whole mount showing the location of the three facial regions marked in (**b**). (1) nasal & medial (med.) canthus region; (2) lateral (lat.) canthus & anterior (ant.) auricular region; and (3) cheek and chin region. Facial skin was removed and prepared as a flattened whole mount. Yellow dashed lines mark the boundaries of each of the three regions of skin. White dashed lines outline the border of the eye and external auditory canal (EAC) in the skin whole mount. Medial and lateral canthus regions were divided using the pupil as the landmark. Anterior and posterior auricular regions were divided using the external auditory canal (EAC) as a landmark. Cheek and chin regions were divided along a line connecting the lowest margin of the eyeball and the external auditory canal. Submandibular lymph node (smLN). Accessory submandibular lymph node (asmLN). Parotid lymph node (ptLN). Scale bar, 1 mm. Representative of $n = 7$ mice from three independent experiments.

d, Fluorescence images obtained 15 min after intradermal infusion of TMR-dextran (red) into each of the three facial skin regions showing the infusion site (red arrowheads) and draining lymphatic (upper panels) and TMR-dextran fluorescence in the parotid lymph node (ptLN) outlined by white dashed lines (lower panels). No TMR-dextran fluorescence was evident in the submandibular (smLN) or accessory submandibular (asmLN) lymph node. Scale bar, 500 μm. Representative of $n = 7$ mice from three independent experiments.

e, Comparison of TMR-dextran fluorescence measured in three superficial cervical lymph nodes 15 min after intradermal infusion into the three regions of facial skin of *Prox1*-GFP mice. Values show TMR-dextran fluorescence intensity in the submandibular (smLN), accessory submandibular (asmLN), and parotid (ptLN) lymph nodes after infusion into each facial region. Each dot is the value for one mouse. $n = 7$ mice from three independent experiments. Error bars indicate mean ± s.e.m. a.u., arbitrary unit. *P* values calculated by Brown-Forsythe ANOVA tests followed by two-tailed Dunnett's T3 multiple comparison post hoc test.

Anatomical positions are indicated in the top left corner: S, superior; I, inferior; A, anterior; P, posterior; M, medial; L, lateral.

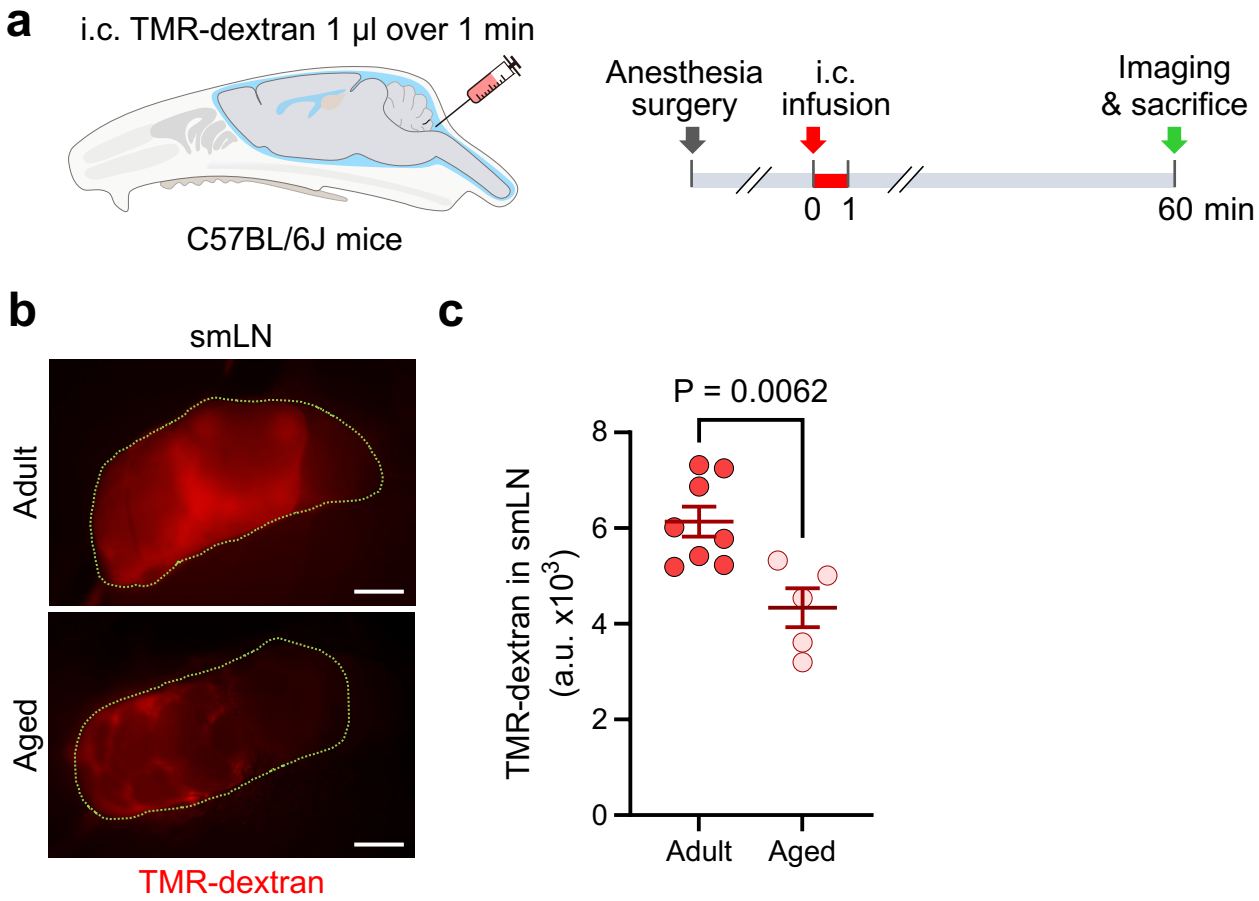

Supplementary Fig. 12. Ageing-related reduction in CSF drainage to the submandibular lymph node

a, Sequence of intracisternal (i.c.) infusion of 1.0 µl TMR-dextran over 1 min into aged and younger adult C57BL/6J mice followed by imaging of TMR-dextran fluorescence in the submandibular lymph node (smLN) 60 min later.

b,**c**, Fluorescence microscopic images and measurements show significantly less TMR-dextran fluorescence in the submandibular lymph node (outlined by green dashed lines) of aged mice (83 weeks) than in younger adults (12 weeks). Scale bars, 500 µm. Each dot is the value for one mouse. *n* = 8 mice for adult, *n* = 5 mice for aged per group from three independent experiments. Error bars indicate mean ± s.e.m. a.u., arbitrary unit. *P* value was calculated by two-tailed Mann-Whitney *U*-tests.

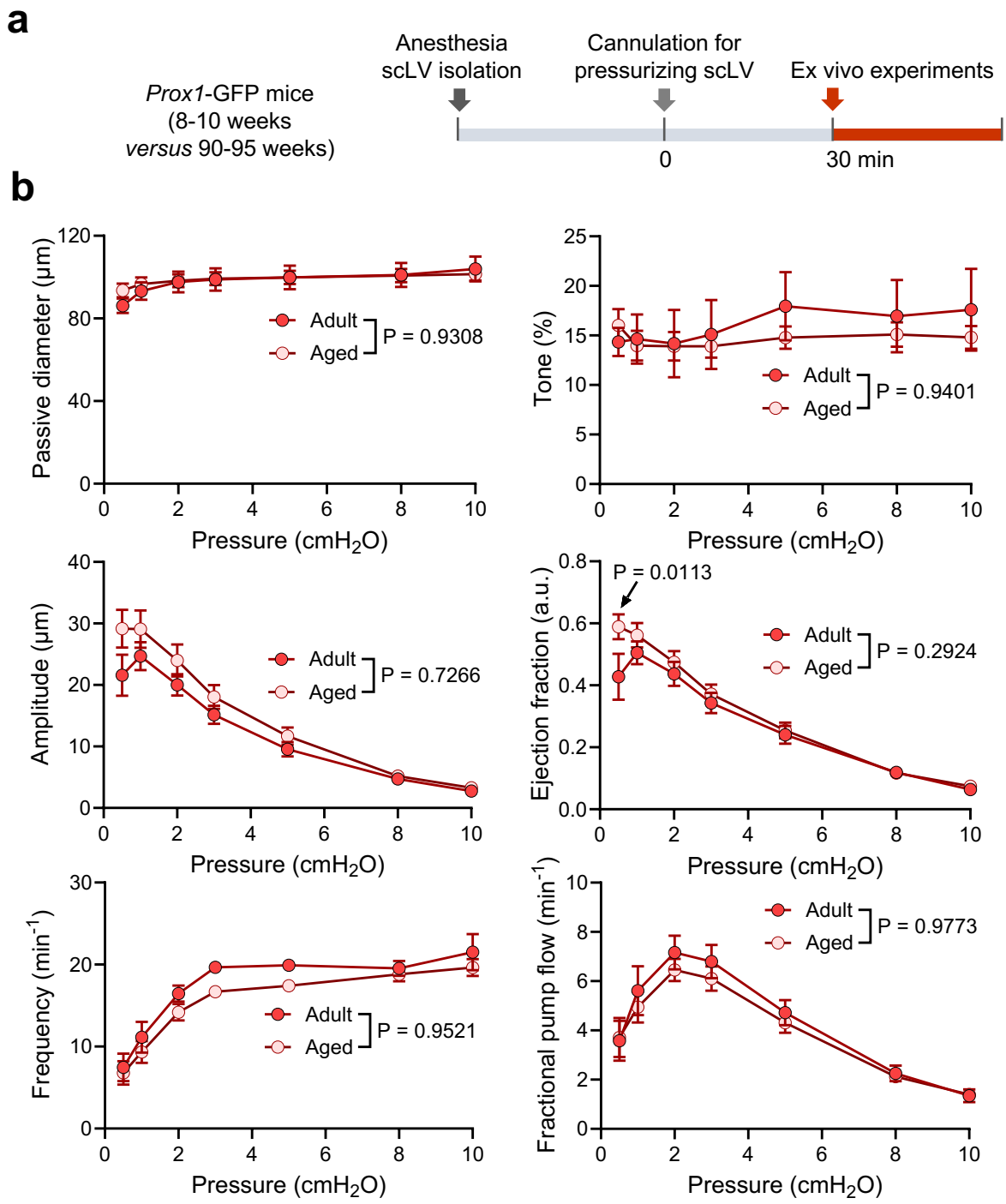

Supplementary Fig. 13. Little or no ageing-related difference in responses to pressure changes in superficial cervical lymphatics *ex vivo*

a, Sequence of *ex vivo* experiments where superficial cervical lymphatics scLV-1 or scLV-2 of adult (8-10 weeks) and aged *Prox1*-GFP mice (90-95 weeks) were isolated, cannulated, and pressurized, and then vessel diameter and spontaneous contractions were measured.

b, Measurements made over physiological pressure range (0.5 to 10 cmH_2O) showing little or no significant age-related differences in passive diameter, tone, amplitude, ejection fraction, frequency and fractional pump flow of scLV-1 or scLV-2 from adult (8-10 weeks) and aged *Prox1*-GFP mice (90-95 weeks). Only the ejection fraction at 0.5 cmH_20 was significantly different in aged mice. Each dot is the value for one mouse. n = 9 mice for adult (8-10 weeks) and n = 14 mice for aged (90-95 weeks) of both sexes from three independent experiments. Error bars indicate mean ± s.e.m. a.u., arbitrary unit. P values calculated by two-way ANOVA test followed by two-tailed Sidak's multiple comparison test.

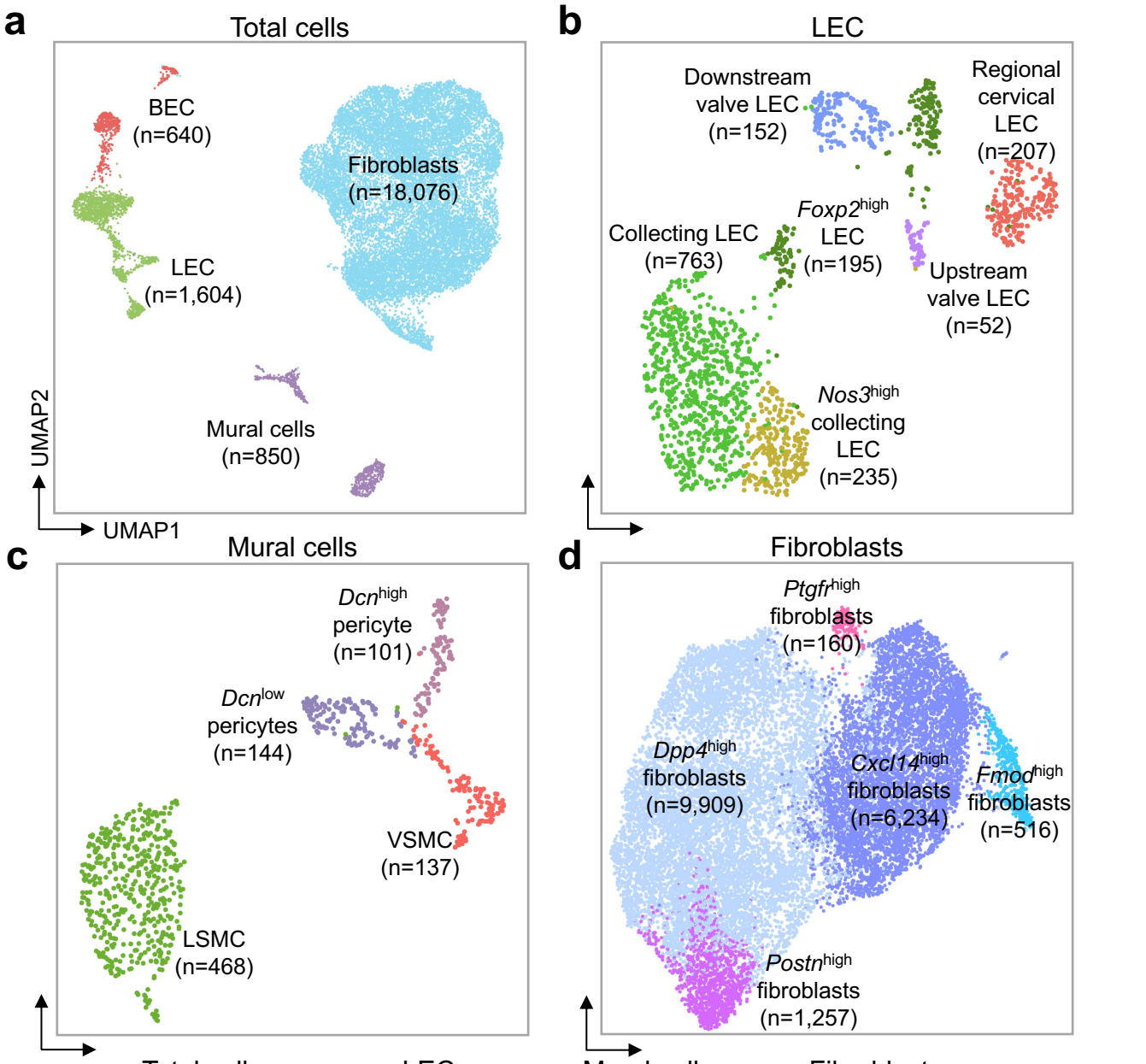
a
Total cells
BEC
(n=640)
Fibroblasts
(n=18,076)
LEC
(n=1,604)
Mural cells
(n=850)
UMAP2
UMAP1
b
LEC
Downstream
valve LEC
(n=152)
Regional
cervical
LEC
(n=207)
Foxp2high
LEC
(n=195)
Collecting LEC
(n=763)
Upstream
valve LEC
(n=52)
Nos3high
collecting
LEC
(n=235)
c
Mural cells
Dcnhigh
pericyte
(n=101)
Dcnlow
pericytes
(n=144)
VSMC
(n=137)
LSMC
(n=468)
d
Fibroblasts
Ptgfrhigh
fibroblasts
(n=160)
Dpp4high
fibroblasts
(n=9,909)
Cxcl14high
fibroblasts
(n=6,234)
Fmodhigh
fibroblasts
(n=516)
Postnhigh
fibroblasts
(n=1,257)
e
Total cells
Col1a2
Pdgfra
Pdgfrb
Vtn
Myh11
Tagln
Acta2
Pecam1
Prox1
LEC
BEC
Mural
Fibroblasts
LEC
Adm
Gja4
Neo1
Cldn11
Piezo2
Reln
Lyve1
Ccl21a
Foxp2
Nos3
Sparc
Procr
Plvap
Fabp4
Eng
Bgn
Apoe
Collecting
Nos3high
Foxp2high
Regional cervical
Up valve
Down valve
Mural cells
Pdgfrb
Vtn
Dcn
Scn3a
Nr4a2
Tagln
Myh11
Acta2
LSMC
VSMC
Dcnhigh pericytes
Dcnlow pericytes
Fibroblasts
Fmod
Sfrp1
Ptgfr
Cxcl14
Cxcl12
Sema3a
Postn
Dpp4
Dpp4high
Postnhigh
Cxcl14high
Ptgfrhigh
Fmodhigh
Average expression
Percent Expressed

Supplementary Fig. 14. Cellular heterogeneity and subsets of superficial cervical lymphatics and surrounding tissues

a-d, Uniform manifold approximation and projection (UMAP) plot of single-cell gene expression (scRNA-seq) analysis identified four subclusters of cells from superficial cervical lymphatics and surrounding tissues from six adult (12 weeks) and six aged (93 weeks) *Prox1*-GFP mice (**a**). The plots show subclusters of lymphatic endothelial cells (LEC, *n* = 1,604), blood vascular endothelial cells (BEC, n = 640), mural cells (*n* = 850), and fibroblasts (*n* = 18,076). Total number of cells analyzed is 21,170. Subclusters of lymphatic endothelial cells (**b**), mural cells (**c**), and fibroblasts (**d**) are shown separately.

e, Dot plots comparing average expression level of multiple genes across subclusters in lymphatic endothelial cells (LEC), mural cells, fibroblasts, and total cells group. In each group, the average expression is indicated by different colors: yellow for total cells, green for LEC, red for mural cells, and blue for fibroblasts.

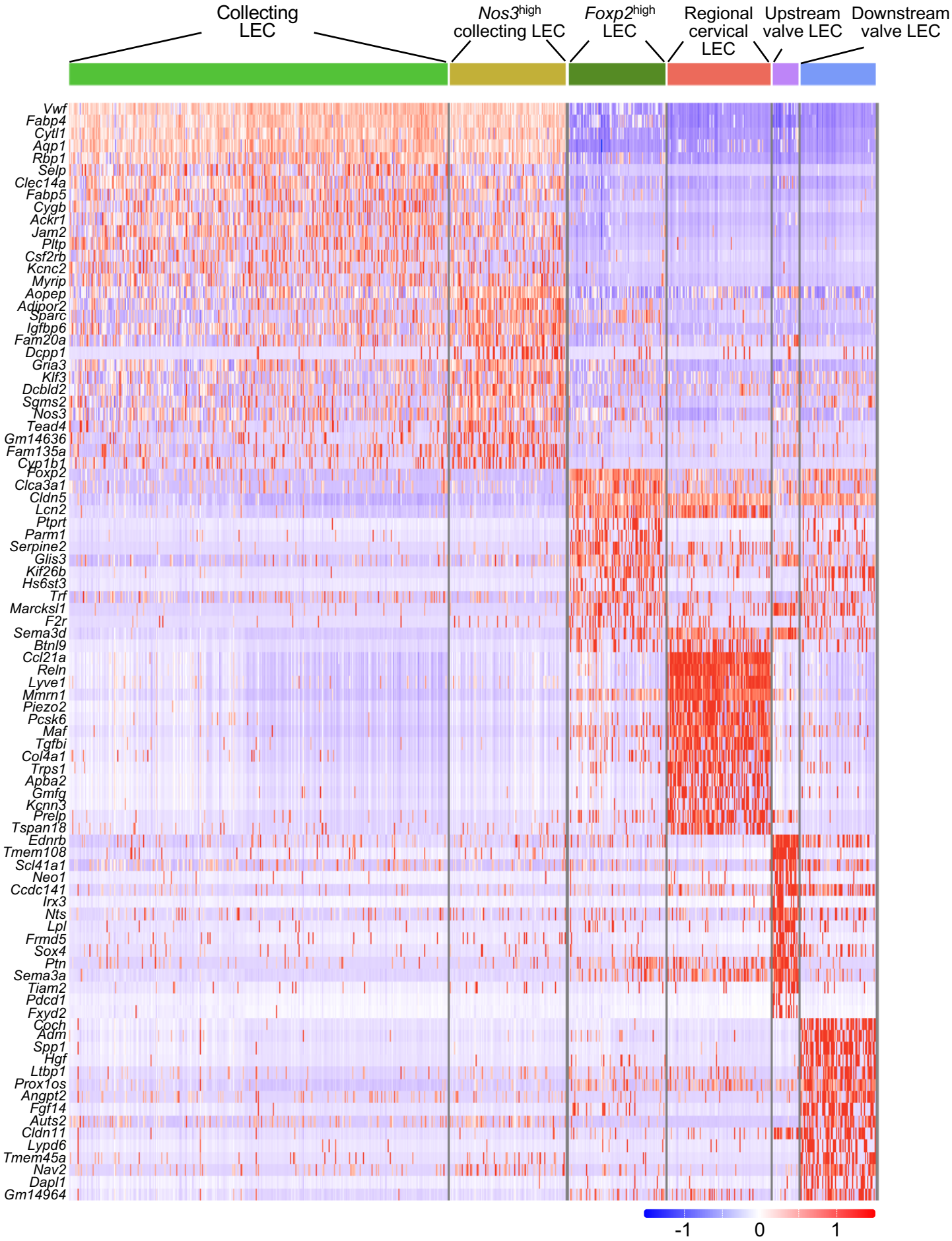
Collecting LEC
Nos3high collecting LEC
Foxp2high LEC
Regional cervical LEC
Upstream valve LEC
Downstream valve LEC
Vwf
Fabp4
Cytl1
Aqp1
Rbp1
Selp
Clec14a
Fabp5
Cygb
Ackr1
Jam2
Pltp
Csf2rb
Kcnc2
Myrip
Aopep
Adipor2
Sparc
Igfbp6
Fam20a
Dcpp1
Gria3
Klf3
Dcbld2
Sgms2
Nos3
Tead4
Gm14636
Fam135a
Cyp1b1
Foxp2
Clca3a1
Cldn5
Lcn2
Ptprt
Parm1
Serpine2
Glis3
Kif26b
Hs6st3
Trf
Marcksl1
F2r
Sema3d
Btnl9
Ccl21a
Reln
Lyve1
Mmrn1
Piezo2
Pcsk6
Maf
Tgfbi
Col4a1
Trps1
Apba2
Gmfg
Kcnn3
Prelp
Tspan18
Ednrb
Tmem108
Scl41a1
Neo1
Ccdc141
Irx3
Nts
Lpl
Frmd5
Sox4
Ptn
Sema3a
Tiam2
Pdcd1
Fxyd2
Coch
Adm
Spp1
Hgf
Ltbp1
Prox1os
Angpt2
Fgf14
Auts2
Cldn11
Lypd6
Tmem45a
Nav2
Dapl1
Gm14964
-1
0
1

Supplementary Fig. 15. Heat map of scRNA-seq analysis showing differentially expressed genes in six lymphatic endothelial cell subclusters

Heat map of scRNA-seq analysis of cells from superficial cervical lymphatics and surrounding tissues from six adult (12 weeks) and six aged (93 weeks) *Prox1*-GFP mice showing differentially expressed genes in the six lymphatic endothelial cell (LEC) subclusters, collecting LEC, *Nos3*^{high} collecting LEC, *Foxp2*^{high} LEC, regional cervical LEC, upstream valve LEC, and downstream valve LEC of superficial cervical lymphatics. Data and statistics for the heat map for LEC are presented in **Supplementary Table 4**.

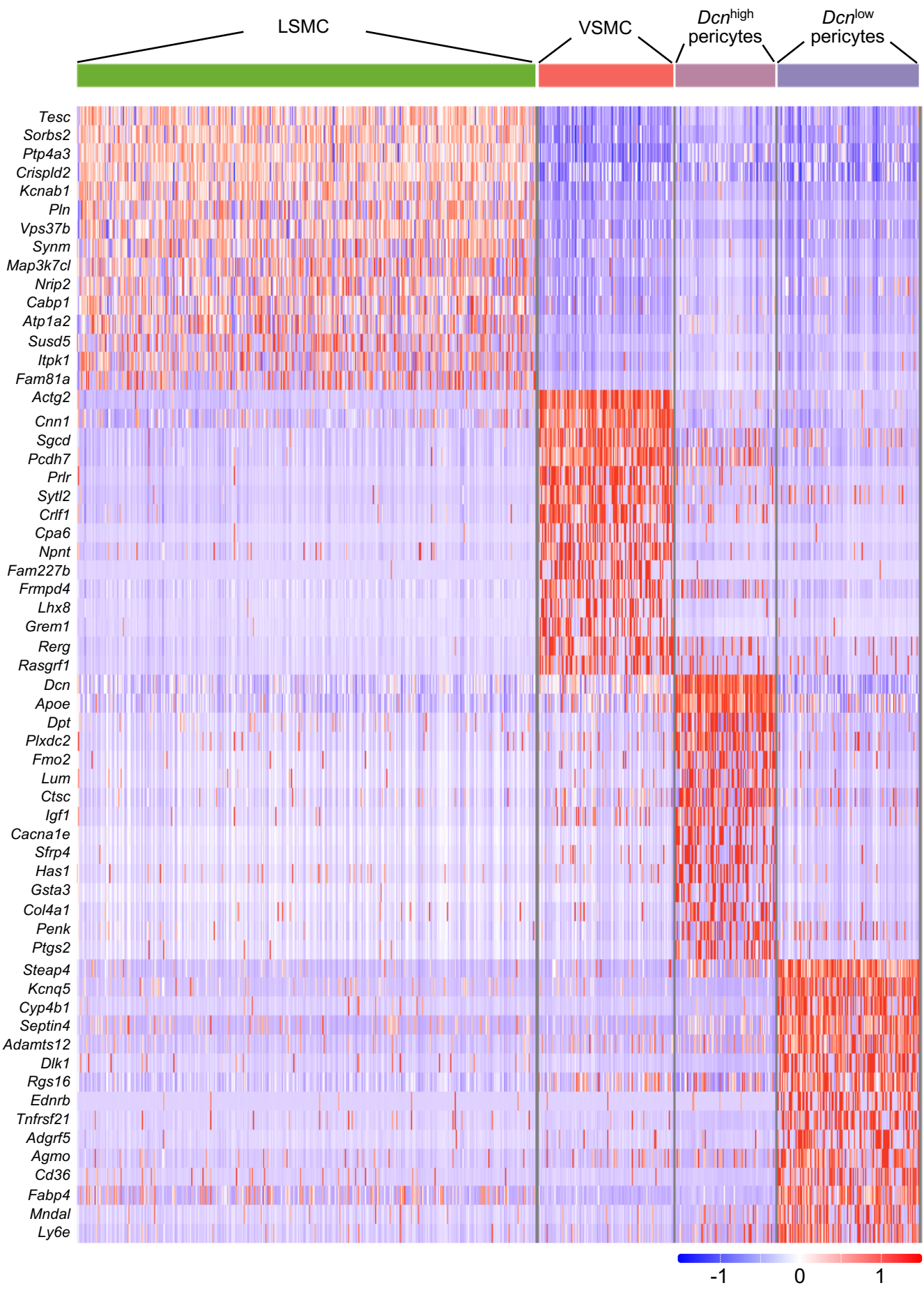
LSMC
VSMC
Dcn^high pericytes
Dcn^low pericytes
Tesc
Sorbs2
Ptp4a3
Crispld2
Kcnab1
Pln
Vps37b
Synm
Map3k7cl
Nrip2
Cabp1
Atp1a2
Susd5
Itpk1
Fam81a
Actg2
Cnn1
Sgcd
Pcdh7
Prlr
Sytl2
Crlf1
Cpa6
Npnt
Fam227b
Frmpd4
Lhx8
Grem1
Rerg
Rasgrf1
Dcn
Apoe
Dpt
Plxdc2
Fmo2
Lum
Ctsc
Igf1
Cacna1e
Sfrp4
Has1
Gsta3
Col4a1
Penk
Ptgs2
Steap4
Kcnq5
Cyp4b1
Septin4
Adamts12
Dlk1
Rgs16
Ednrb
Tnfrsf21
Adgrf5
Agmo
Cd36
Fabp4
Mndal
Ly6e
-1
0
1

Supplementary Fig. 16. Heat map of scRNA-seq analysis showing differentially expressed genes in four mural cell subclusters

Heat map of scRNA-seq analysis of cells from superficial cervical lymphatics and surrounding tissues from six adult (12 weeks) and six aged (93 weeks) *Prox1*-GFP mice showing differentially expressed genes in four mural cell subclusters, representing lymphatic smooth muscle cells (LSMC), blood vascular smooth muscle cells (VSMC), *Dcn*^{high} pericytes, and *Dcn*^{low} pericytes. Data and statistics for the heat map for mural cells are presented in **Supplementary Table 5**.

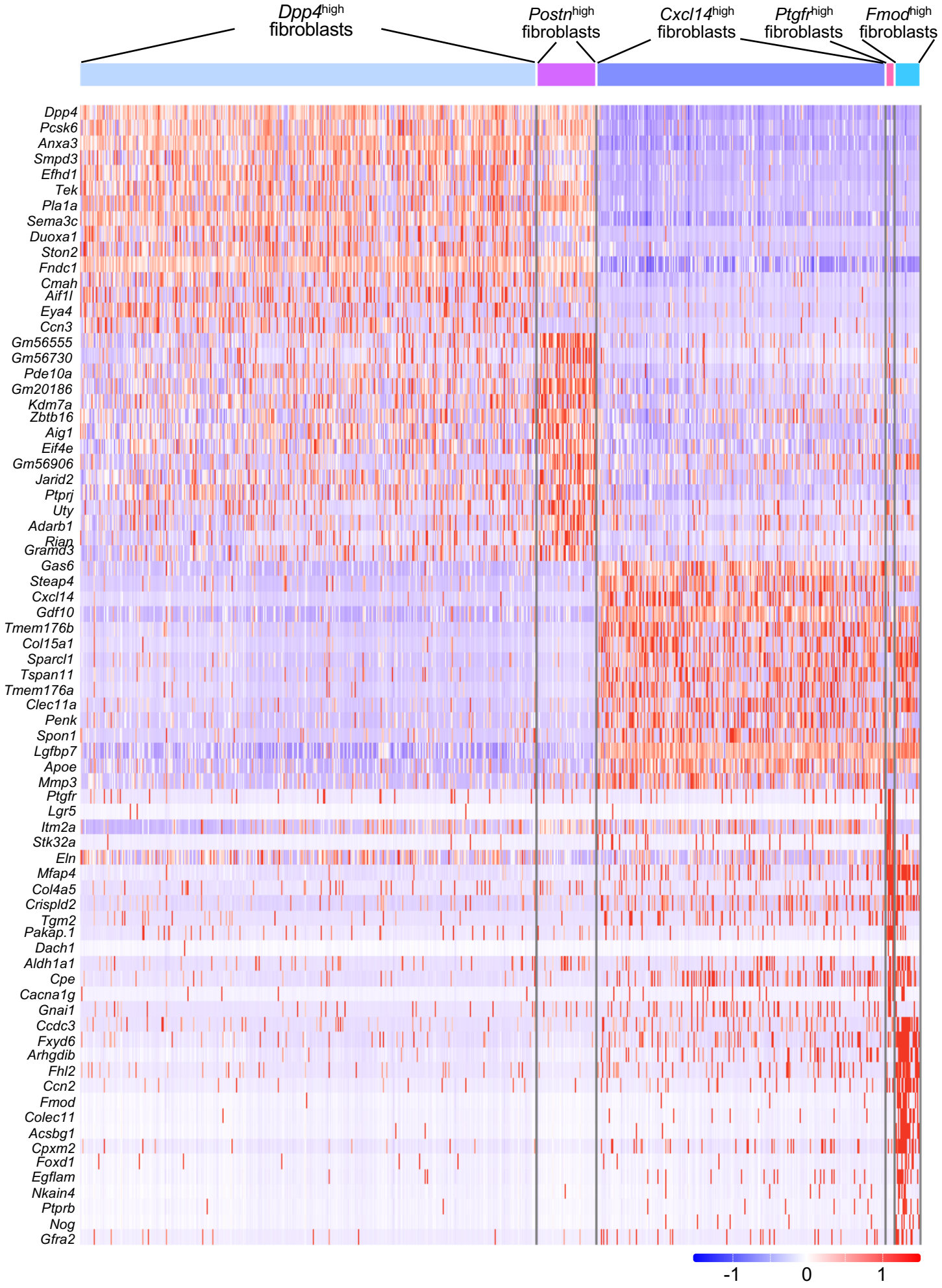
Dpp4high fibroblasts
Postnhigh fibroblasts
Cxcl14high fibroblasts
Ptgfrhigh fibroblasts
Fmodhigh fibroblasts
Dpp4
Pcsk6
Anxa3
Smpd3
Efhd1
Tek
Pla1a
Sema3c
Duoxa1
Ston2
Fndc1
Cmah
Aif1l
Eya4
Ccn3
Gm56555
Gm56730
Pde10a
Gm20186
Kdm7a
Zbtb16
Aig1
Eif4e
Gm56906
Jarid2
Ptprj
Uty
Adarb1
Rian
Gramd3
Gas6
Steap4
Cxcl14
Gdf10
Tmem176b
Col15a1
Sparcl1
Tspan11
Tmem176a
Clec11a
Penk
Spon1
Lgfbp7
Apoe
Mmp3
Ptgfr
Lgr5
Itm2a
Stk32a
Eln
Mfap4
Col4a5
Crispld2
Tgm2
Pakap.1
Dach1
Aldh1a1
Cpe
Cacna1g
Gnai1
Ccdc3
Fxyd6
Arhgdib
Fhl2
Ccn2
Fmod
Colec11
Acsbg1
Cpxm2
Foxd1
Egflam
Nkain4
Ptprb
Nog
Gfra2
-1
0
1

Supplementary Fig. 17. Heat map of scRNA-seq analysis showing differentially expressed genes in five fibroblast subclusters

Heat map of scRNA-seq analysis of fibroblasts around superficial cervical lymphatics from six adult (12 weeks) and six aged (93 weeks) *Prox1*-GFP mice showing differentially expressed genes in the five fibroblasts subclusters: *Dpp4*^{high} fibroblasts, *Postn*^{high} fibroblasts, *Cxcl14*^{high} fibroblasts, *Ptgfr*^{high} fibroblasts, and *Fmod*^{high} fibroblasts. Data and statistics for the heat map for fibroblasts are presented in **Supplementary Table 6**.

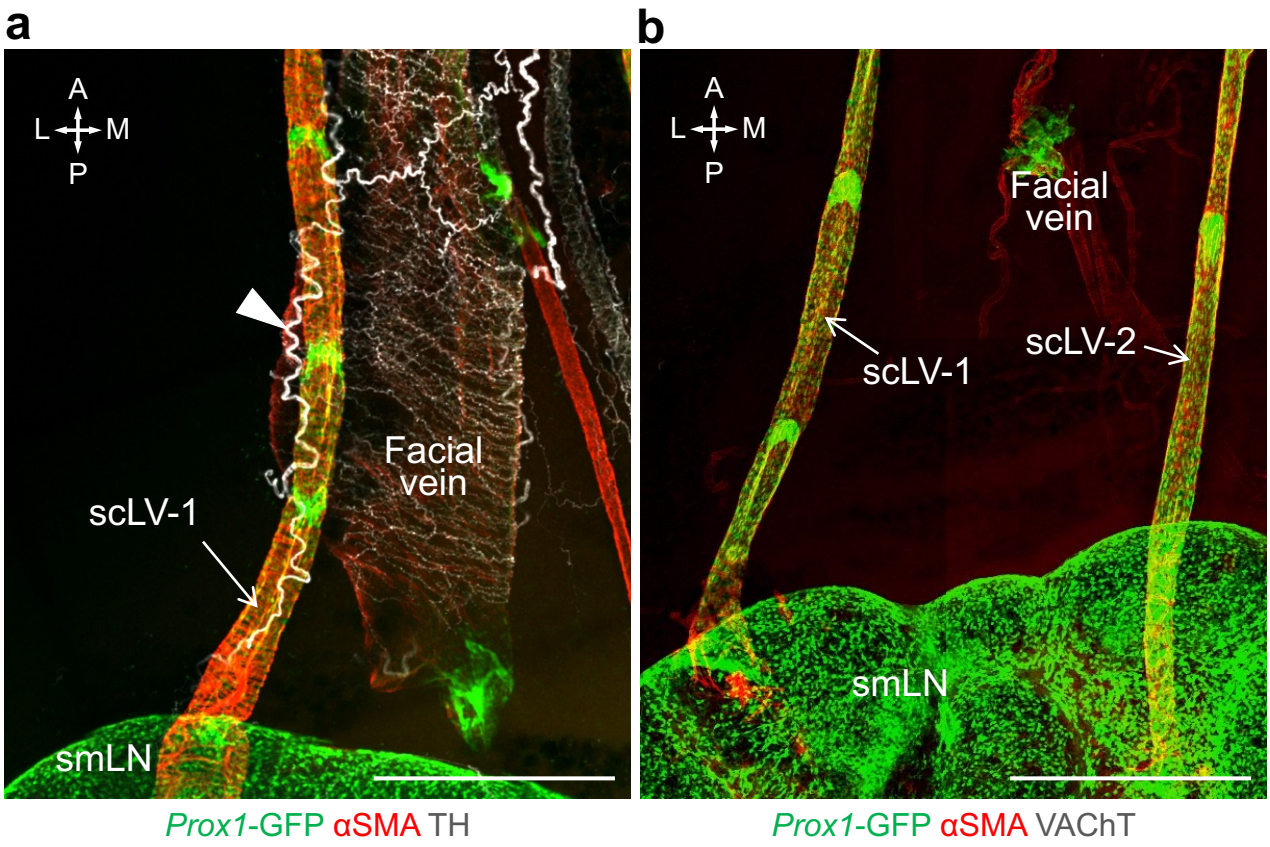

Supplementary Fig. 18. Adrenergic innervation but not cholinergic innervation of superficial cervical lymphatics

a,b, Immunofluorescence images of whole mounts of superficial cervical lymphatics in adult *Prox1*-GFP mice showing the presence of tyrosine hydroxylase $(TH)^+$ adrenergic axons (white arrowhead) running along scLV-1 (**a**) and absence of vesicular acetylcholine transporter $(VAChT)^+$ cholinergic axons near scLV-1 and scLV-2 (**b**). Both lymphatics have uniform coverage by circular smooth muscle cells (α-smooth muscle actin, αSMA, red). Anatomical positions are indicated in the top left corner: A, anterior; P, posterior; M, medial; L, lateral. Scale bars, 500 μm. Representative of *n* = 6 mice from three independent experiments.

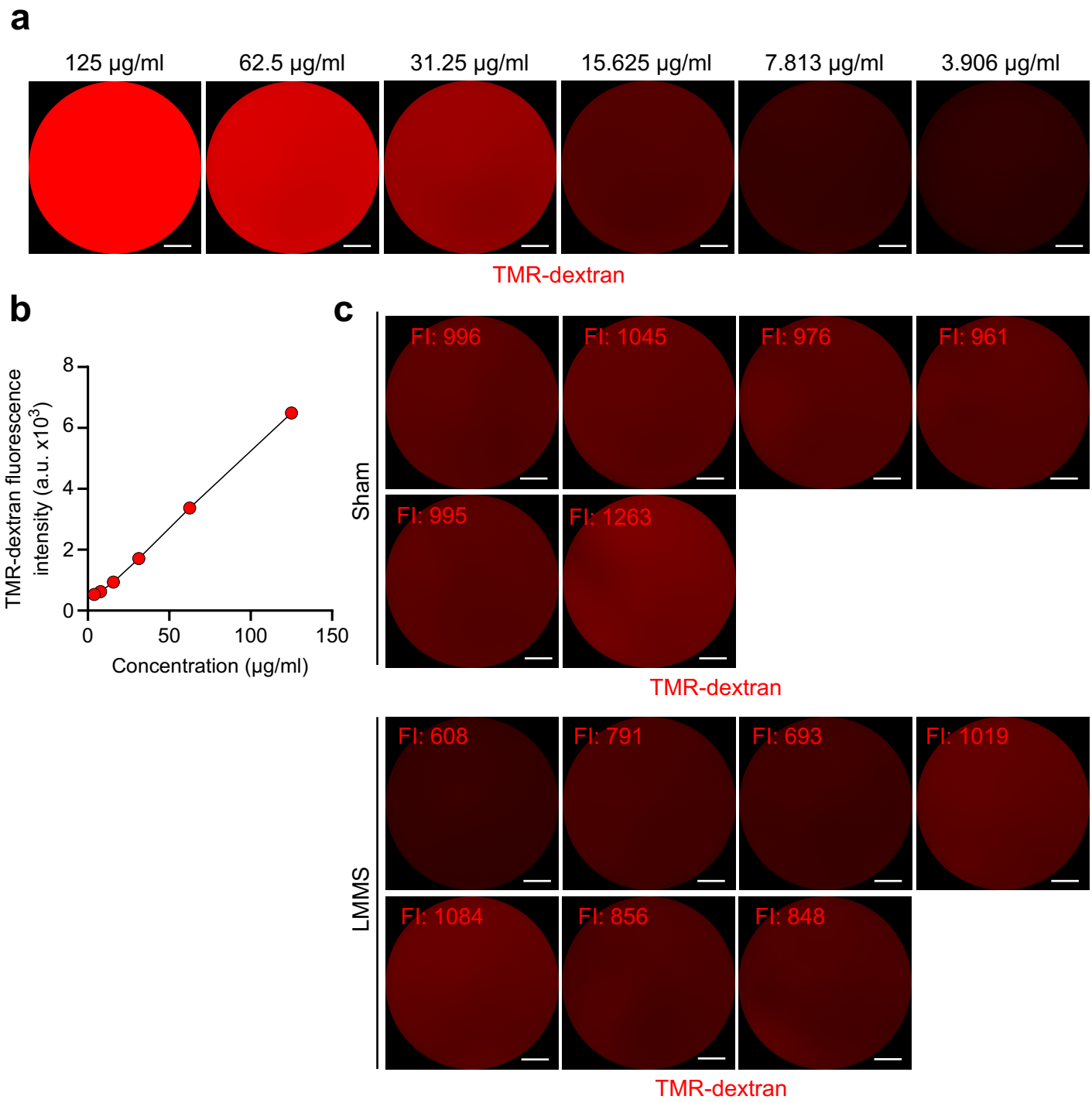

Supplementary Fig. 19. Measurement and comparison of TMR-dextran fluorescence of CSF after low-magnitude mechanical stimulation on superficial cervical lymphatics

a, Images showing the diminishing fluorescence of serial dilutions of TMR-dextran concentrations ranging from 125.000 µg/ml to 3.906 µg/ml. Scale bars, 1 mm.

b, Graph of the standard curve of fluorescence intensity as a function of TMR-dextran concentration over the range shown in (**a**). Fluorescence intensity values in **Fig. 6h** fit within this range of TMR-dextran concentrations.

c, Images showing the raw fluorescence intensity data for each Sham group and each low-magnitude stimulation (LMMS) group, as presented in **Fig. 6h**.

Supplementary Table 1 (related to Extended Data Fig. 10c)

A list of genes filtered by absolute avg_log2FC values greater than 0.3. Positive values of avg_log2FC indicate genes more highly expressed in the aged group, while negative values represent genes more highly expressed in the adult group.

Gene	p_val	avg_log2FC	pct.1	pct.2	p_val_adj
H2-Q7	8.27370517732052E-37	-0.518715467915018	0.345	0.636	1.94605819475756E-32
H2-Q6	5.61542111775348E-35	-0.774301997087943	0.219	0.491	1.3208032011068E-30
H2-Q4	2.9560691208673E-30	-0.470880863878659	0.309	0.556	6.95297017919197E-26
B2m	4.54582554473468E-30	-0.493348836520625	0.94	0.978	1.06922362637704E-25
Gsn	1.30779337199024E-27	0.455378865876228	0.522	0.665	3.07606079025824E-23
Rpl29	6.26276844430736E-27	-0.33903604115654	0.453	0.696	1.47306576578553E-22
Aopep	1.27768824920867E-26	0.656197330098268	0.706	0.753	3.00525053096371E-22
Psmb9	1.04838704136825E-25	-0.362483264450828	0.324	0.546	2.46591116000227E-21
Bst2	2.07219519415516E-25	-0.58529821493786	0.438	0.699	4.87401031617236E-21
Adipor2	2.82883154579506E-25	0.763588222921752	0.452	0.466	6.65369467886456E-21
Uba52	5.06940351260064E-25	-0.325295382562566	0.309	0.51	1.1923744001988E-20
Eif2s2	7.79842269923236E-25	0.371528461638921	0.552	0.627	1.83426700308644E-20
H2-T23	1.88119757885044E-24	-0.535074840481649	0.54	0.791	4.42476482521413E-20
Cbx3	1.25881583748228E-23	-0.424433862657791	0.235	0.42	2.96086073134206E-19
Cystm1	4.98746520761933E-23	-0.615489360512903	0.149	0.323	1.17310169148414E-18
Alkbh5	1.01635877348399E-21	-0.360833549940412	0.233	0.403	2.39057747111168E-17
H2-D1	1.78729175294634E-21	-0.387006307089896	0.992	0.992	4.2038889321051E-17
Parvb	2.81026531313169E-21	0.502993614942635	0.363	0.405	6.61002504301705E-17
mt-Nd3	4.57177825310171E-21	-0.301603260123067	0.576	0.791	1.07532796291205E-16
Ssr2	5.66531040974085E-21	0.42794008684438	0.292	0.332	1.33253766147514E-16
Elk4	5.99081511401206E-21	-0.31025353034818	0.322	0.509	1.40909962296678E-16
Rpl35a	8.90723022960888E-21	-0.39530777407919	0.953	0.981	2.09506962230631E-16
Cstb	1.40086002456798E-20	-0.346298688153077	0.194	0.346	3.29496286378634E-16
Slc66a2	1.90303038465397E-20	0.393139694152198	0.536	0.592	4.4761177677446E-16
Snhg8	2.17492322761891E-20	-0.43963520124601	0.227	0.405	5.11563692368243E-16
Cyc1	3.07022801256233E-20	0.392328106470034	0.32	0.365	7.22148330834785E-16
Arl6ip5	3.77193493120499E-20	0.403202050455367	0.492	0.546	8.87196815168726E-16
Immt	4.22537622743761E-20	0.346574859653545	0.302	0.354	9.938507424556E-16
Rps27	8.74078636213735E-20	-0.382194167070812	0.946	0.978	2.05592036023833E-15
Cox17	1.11761330094983E-19	-0.366824906379581	0.27	0.446	2.6287382451641E-15
Acvrl1	1.42455703478121E-19	0.311979412099853	0.508	0.576	3.35070060150887E-15
Nek7	1.53452886435654E-19	0.326692372580977	0.531	0.63	3.60936534185301E-15
Fos	4.14404016544701E-19	-0.432565324555364	0.736	0.907	9.74719687314791E-15
Pkn3	9.83631676971353E-19	0.31903186011399	0.31	0.362	2.31360006740432E-14
Capg	1.05097131130902E-18	0.393698145721919	0.343	0.395	2.47198962132994E-14

Ninj1	1.12681887916696E-18	0.333895068359313	0.462	0.521	2.6503906856886E-14
Eif1b	1.3161070996949E-18	-0.359758853613381	0.234	0.392	3.09561550919238E-14
Ctnnal1	3.02629551567679E-18	0.479602895005317	0.556	0.589	7.11814968242338E-14
2410006H16Rik	5.20829316647905E-18	-0.38260442195964	0.369	0.572	1.22504263568754E-13
Egr1	5.44488974018718E-18	-0.510074097663503	0.708	0.882	1.28069251578943E-13
Btg2	9.29360640973922E-18	-0.519163985800868	0.725	0.883	2.18594916363476E-13
Mall	1.21874918545796E-17	0.30959885064547	0.395	0.455	2.86661995911567E-13
Usp24	1.83929815445304E-17	0.324831766120376	0.327	0.386	4.32621318908899E-13
Sparc	2.12299918173402E-17	1.03948166973571	0.417	0.321	4.99350637535658E-13
Fuca1	2.29591774076031E-17	0.33730884824826	0.418	0.472	5.40022811804233E-13
Synpo	2.62713367437736E-17	0.386370730721701	0.47	0.512	6.17928111550298E-13
Rps28	2.84499683600082E-17	-0.392324656243365	0.936	0.959	6.69171705795752E-13
Tpm1	3.79222345980229E-17	0.328597279805161	0.367	0.427	8.91968879980097E-13
Rfk	4.01262340189188E-17	0.322385631012685	0.504	0.564	9.43809150358988E-13
S1pr1	5.52172220378475E-17	0.333724973946681	0.655	0.721	1.29876427955221E-12
Rnf10	7.15419339359753E-17	-0.351250795194515	0.311	0.479	1.68273782810808E-12
Lamb2	1.13258272089992E-16	0.400860762588342	0.44	0.476	2.6639478178287E-12
Ano6	1.90031397285375E-16	0.339065445162346	0.379	0.433	4.46972849554931E-12
Epb41	2.12010536963105E-16	0.301728658967248	0.302	0.365	4.9866998399092E-12
Dcbld2	2.64651868201548E-16	0.528111045873177	0.425	0.45	6.22487659196861E-12
Tbc1d15	3.07260931414207E-16	0.39655724781215	0.358	0.391	7.22708436779357E-12
Dpysl2	3.31789140731938E-16	-0.368499052497882	0.27	0.431	7.80401237915591E-12
Rpl37a	3.40489394424989E-16	-0.334935448972884	0.969	0.983	8.00865104627017E-12
Rps21	3.59828937954256E-16	-0.320198039843453	0.978	0.989	8.46353644962206E-12
Rpl37	4.0279008141418E-16	-0.35338430973922	0.939	0.972	9.47402550494294E-12
Serpina1d	4.32656789172979E-16	0.76679569052868	0.376	0.346	1.01765203381376E-11
Klf3	7.14548482449994E-16	0.657548122724178	0.51	0.531	1.68068948557063E-11
Cgnl1	8.24946579946199E-16	0.344592644073183	0.369	0.428	1.94035685069145E-11
Psmd13	9.76568331225825E-16	0.339785799888952	0.261	0.304	2.29698637187626E-11
Adcy4	9.8101626338111E-16	0.344400169043272	0.396	0.441	2.30744835309871E-11
Hnrnpl	1.11756631084244E-15	0.394049120765328	0.295	0.339	2.6286277197325E-11
Snap23	2.03941949218823E-15	0.363840743690578	0.301	0.339	4.79691858757594E-11
Tnfrsf12a	2.7842164128668E-15	0.479805059787308	0.378	0.409	6.54875542470401E-11
Flnb	3.74403085229828E-15	0.389632322225314	0.7	0.748	8.80633496769078E-11
Zdhhc20	4.14072720291026E-15	0.338728289185432	0.342	0.398	9.73940445396523E-11
Psen2	4.46536831564776E-15	0.320665959176015	0.567	0.614	1.05029928152351E-10
H2-K1	4.84299902649287E-15	-0.378539563576283	0.933	0.965	1.13912180102139E-10
Nos3	6.22350696539753E-15	0.384693349934788	0.54	0.602	1.46383107333115E-10
Ssbp2	6.72877675523378E-15	-0.352278526805451	0.298	0.46	1.58267558059854E-10
Met	7.49308004634727E-15	0.644889286668033	0.366	0.369	1.76244735770134E-10
Tnfsf10	8.02431063079796E-15	-0.354729696969409	0.189	0.32	1.88739810346999E-10

Mt1	8.6919249532212E-15	0.664863934529113	0.386	0.469	2.04442766824716E-10
Emp2	1.217111876862E-14	0.413095597016298	0.304	0.342	2.86276884556712E-10
Mob2	1.49181766607928E-14	0.310083639783112	0.251	0.304	3.50890433238508E-10
Rpl39	1.85605325381903E-14	-0.361023192759898	0.907	0.962	4.36562285830774E-10
Ndufb1	1.91932957636179E-14	-0.397106173611204	0.218	0.359	4.51445509656058E-10
Herpud1	2.46448672010712E-14	0.324543807545662	0.525	0.57	5.79671921436396E-10
Cops9	6.76813137097797E-14	-0.36727884787965	0.189	0.313	1.59193217976773E-09
Ikbkb	6.9722481549597E-14	0.318579037108686	0.267	0.318	1.63994248852807E-09
Acot9	7.07991963852369E-14	0.30901628620557	0.3	0.348	1.66526789817716E-09
St3gal6	7.25145173135379E-14	0.420403206324736	0.469	0.512	1.70561396173172E-09
Klhl4	8.026503004224E-14	-0.322017121992389	0.425	0.603	1.88791377162353E-09
Sod2	8.25722484775963E-14	0.39438985649592	0.296	0.321	1.94218185644154E-09
Vps4b	8.52529579302333E-14	0.32410345896936	0.264	0.307	2.00523482347702E-09
Stk40	8.79245729149763E-14	0.332998644111107	0.27	0.306	2.06807387953316E-09
Anxa2	9.81867211261324E-14	0.332031889397033	0.882	0.932	2.30944986760776E-09
H2-Ab1	1.61733032269182E-13	-0.453833184840737	0.187	0.331	3.80412265200343E-09
Ppp2r3a	1.79206105816917E-13	0.367917939524218	0.363	0.409	4.21510681491971E-09
Avpi1	2.36082698556756E-13	0.55180096518937	0.395	0.408	5.55290115275347E-09
Cd55	2.62950975643639E-13	0.520411571798438	0.312	0.34	6.18486989811403E-09
Oga	2.64692765125524E-13	0.348314314238258	0.305	0.343	6.22583852851744E-09
Gria3	2.75793482684436E-13	0.361066791415469	0.492	0.528	6.48693850622061E-09
Alyref	3.4403795189816E-13	-0.317129278450222	0.186	0.301	8.09211666659661E-09
Lrrc1	3.73708854966369E-13	0.382088735884127	0.263	0.302	8.79000597766396E-09
Nars	3.85483861792119E-13	0.417797912033188	0.311	0.328	9.06696591321243E-09
Ccdc186	6.1104809744262E-13	0.361394740159654	0.291	0.321	1.43724622999479E-08
Mex3c	6.233721788867E-13	-0.326553961536947	0.195	0.315	1.46623370195941E-08
Slc39a1	6.40198978468246E-13	-0.341578821880896	0.202	0.331	1.50581201725516E-08
Fam20a	7.05966922805381E-13	0.789585204072426	0.413	0.386	1.66050479913054E-08
Ndufc1	7.62449818857723E-13	-0.420170673320736	0.285	0.441	1.79335821893525E-08
Tmem158	9.25236446528197E-13	0.42476003224409	0.628	0.641	2.17624864587897E-08
Kctd12	1.18211433605396E-12	-0.474319340108486	0.277	0.435	2.78045112983252E-08
Orai1	1.26284756310326E-12	0.355578233862635	0.286	0.317	2.97034375317518E-08
Raf1	1.83868293407484E-12	-0.311692031232903	0.232	0.364	4.32476612923744E-08
Mir22hg	1.92552078003305E-12	0.333249707949583	0.337	0.376	4.52901742671573E-08
Zfhx3	2.36408650026365E-12	-0.324507140502813	0.352	0.509	5.56056785727014E-08
Ier2	2.704618766195E-12	-0.347678573320693	0.669	0.83	6.36153379996725E-08
Hs3st1	3.21988593419283E-12	0.303532861574612	0.519	0.578	7.57349370581495E-08
Rhob	5.1993057178135E-12	-0.349087105698014	0.324	0.487	1.22292869788691E-07
Anxa3	6.22558329059927E-12	0.356441137106782	0.461	0.488	1.46431944578185E-07
Hes1	6.4646895234722E-12	-0.518231015791289	0.386	0.564	1.5205596228159E-07
Ralgds	1.04059069799593E-11	0.386098151727867	0.286	0.331	2.44757338075622E-07

Rpl31	1.43575382328547E-11	-0.315279098836657	0.816	0.923	3.37703656774976E-07
Grk5	1.43583970192863E-11	0.309120685049281	0.65	0.698	3.37723856290632E-07
Itgb4	2.63486643609944E-11	0.341576800311404	0.514	0.567	6.1974693443495E-07
Pls3	2.71163600289626E-11	0.387727156020242	0.27	0.317	6.37803904241229E-07
Socs3	2.91908542633622E-11	-0.406668365606319	0.504	0.677	6.86598083128543E-07
Tnfrsf1a	3.04233209658204E-11	0.31413235011509	0.572	0.591	7.15586932437062E-07
Lrrc8c	3.05511817543172E-11	0.547435560358082	0.317	0.326	7.18594346043294E-07
Rpl35	3.90668569880248E-11	-0.340342795339595	0.869	0.942	9.1889154321533E-07
Tmem184b	4.28428878433026E-11	0.344603277767891	0.314	0.343	1.00770756496232E-06
Ltbp3	5.04612495428203E-11	0.319547916000374	0.263	0.304	1.18689905049668E-06
Nol10	6.65930952144944E-11	-0.357919528887042	0.221	0.34	1.56633619254012E-06
Sik1	6.96295031340357E-11	-0.315138723434421	0.424	0.587	1.63775554321565E-06
Rpl38	7.16398707583634E-11	-0.30227497040966	0.901	0.959	1.68504140010746E-06
S100a10	7.92106070693098E-11	0.30089871939208	0.932	0.959	1.86311268887724E-06
Tm4sf1	8.30757643258728E-11	0.349333617409487	0.87	0.904	1.95402505270885E-06
Ackr3	9.50431070308262E-11	0.473919688307869	0.595	0.609	2.23550892047206E-06
Igfbp6	1.28758581251408E-10	0.784171512229294	0.533	0.483	3.02853058961436E-06
Ypel2	1.39999182893518E-10	0.470074774169896	0.571	0.572	3.29292078083843E-06
Emp3	1.42829432058121E-10	0.444646736042587	0.431	0.438	3.35949107143905E-06
Slc7a1	1.7792511772251E-10	0.404648076235557	0.442	0.458	4.18497669395116E-06
Fbxo34	3.74855022619258E-10	0.366277044320443	0.364	0.392	8.81696498702757E-06
Adh1	4.91878069941462E-10	0.422109734062441	0.318	0.337	1.15694640830931E-05
Rgs16	5.13485497110438E-10	-0.340175185274858	0.3	0.436	1.20776923775346E-05
Errfi1	6.23253148872286E-10	0.372479633686481	0.453	0.521	1.4659537314625E-05
Ern1	6.54487571141884E-10	0.453101615218896	0.517	0.569	1.53942021608282E-05
Plaur	6.63214938751578E-10	0.55713454709818	0.308	0.302	1.55994785743759E-05
Colec12	8.66710863697539E-10	-0.353274206633009	0.347	0.488	2.03859062250298E-05
Nr3c2	9.49258666654514E-10	-0.456830065773944	0.387	0.542	2.23275130983808E-05
Flt4	1.092553555553E-09	-0.444277886994456	0.244	0.383	2.56979521801622E-05
Apbb2	1.32200793528949E-09	0.340635600032566	0.57	0.581	3.10949486459441E-05
Rpl36a	1.33240245190586E-09	-0.305179668724649	0.866	0.943	3.13394380712778E-05
Ctla2a	1.36088710425749E-09	0.47271447060145	0.812	0.778	3.20094255792404E-05
St3gal1	1.59783470706694E-09	0.31152463661741	0.482	0.528	3.75826701449216E-05
Arl15	1.7856893593327E-09	0.345512201167007	0.611	0.672	4.20011994208644E-05
Gch1	2.28428248569644E-09	0.332517872900272	0.511	0.517	5.3728608346066E-05
Gbp7	2.33721829363411E-09	-0.446309393236349	0.238	0.37	5.4973711484568E-05
Schip1	2.45878230061125E-09	0.395871402208456	0.496	0.509	5.78330184926773E-05
Stard13	2.49393496817206E-09	0.300335081538396	0.601	0.639	5.8659844386375E-05
Tinagl1	3.35228085622186E-09	0.37414233706004	0.467	0.471	7.88489980191945E-05
Cd34	3.40200465008721E-09	0.505787655488337	0.462	0.428	8.00185513747014E-05
Plpp1	3.41230022362554E-09	0.321412539300998	0.57	0.617	8.02607135598962E-05

Klf10	5.46295017506403E-09	0.338595316506359	0.3	0.323	0.000128494051067681
Eeig2	5.48978424557228E-09	-0.351776279962876	0.266	0.392	0.000129125215240106
Sulf1	7.11281323991459E-09	0.576203070491397	0.54	0.499	0.000167300480216031
Mical2	8.79186996319102E-09	0.389456618859664	0.389	0.402	0.000206793573404216
Dlg1	1.19378184533374E-08	-0.392551002632159	0.374	0.515	0.000280789427840949
Cd200	1.40120791277344E-08	0.308365919671342	0.488	0.518	0.000329578113163441
Prox1os	2.19435527531356E-08	-0.438497897520688	0.217	0.34	0.000516134304306503
Ly6a	2.37588230395172E-08	0.402035423551614	0.542	0.542	0.000558831276712485
Fbxl7	2.7011886391515E-08	0.348299292928765	0.522	0.569	0.000635346579814824
Foxp2	2.8848530280778E-08	-0.369400558454211	0.321	0.458	0.000678546280734179
Ehd4	3.6602047776322E-08	0.321596011279038	0.73	0.724	0.00086091676574687
Ctsh	4.77873367474546E-08	0.304301028063627	0.545	0.559	0.00112400594763688
Samd5	5.5767664336457E-08	0.436364420532078	0.355	0.35	0.0013117112328578
Clu	7.47070568797938E-08	0.321409836496601	0.702	0.704	0.00175718468486963
Kank1	1.0090148021563E-07	0.339326280544066	0.547	0.561	0.00237330371615184
Zswim4	1.11728975299552E-07	-0.32164508918769	0.315	0.438	0.00262797722802076
Cdh13	1.28154731113079E-07	0.391734150346631	0.806	0.784	0.00301432743051073
Zfp36	1.41069422769327E-07	-0.429153274173477	0.761	0.858	0.00331809389295733
Lsr	1.44240457579558E-07	0.307925038753035	0.293	0.315	0.00339267980272878
Gclc	1.71196184021634E-07	0.456297375348394	0.332	0.365	0.00402670544437286
Hspa4l	1.98147328933198E-07	0.343314983285935	0.273	0.306	0.00466062332383775
Adgrg3	2.10132410532842E-07	-0.3819078881361	0.211	0.318	0.00494252442814298
Mrtfb	2.45446118186046E-07	0.420248878849275	0.414	0.452	0.00577313814585399
Mcc	2.5276420643643E-07	0.641776418145157	0.286	0.302	0.00594526689959127
Nr4a1	3.38023752511472E-07	-0.385832404613065	0.648	0.765	0.00795065668282233
Esam	7.40699368859328E-07	0.300742666106363	0.631	0.63	0.0174219898549403
Fbln2	8.72857731760149E-07	0.393070639771028	0.515	0.499	0.0205304867087305
Pakap.1	8.93654179660009E-07	0.32067147645855	0.769	0.772	0.0210196399597831
Myof	9.04911007982572E-07	0.389756368186415	0.594	0.578	0.0212844118187581
Spaca6	1.16346744527724E-06	0.352337121873009	0.314	0.32	0.0273659177803659
Bace2	1.38137644283153E-06	0.370234255957061	0.522	0.521	0.0324913553118403
Bcam	1.97187907394825E-06	0.313998344040548	0.535	0.535	0.0463805676983367
Sh3pxd2a	2.03483204998054E-06	0.365539919662923	0.312	0.324	0.0478612846475923

Supplementary Table 2 (related to Extended Data Fig. 10d)

Term	*P* Value	Adjusted *P* Value	Odd Ratio	Combined Score	Genes
Negative Regulation Of Cellular Process (GO:0048523)	8.91E-07	3.21E-04	13.36380821	186.1673077	*Niban2 Nos3 Cyp1b1 Igfbp6 Ccn2 Nupr1 Pthlh Dcbld2*
Negative Regulation Of Cell Population Proliferation (GO:0008285)	1.80E-05	0.003237057	13.1347185	143.510557642425	*Niban2 Nos3 Cyp1b1 Igfbp6 Nupr1 Pthlh*
Nitric Oxide Biosynthetic Process (GO:0006809)	2.26E-04	0.018548352 4946417	109.6538461 53846	920.723866271055	*Nos3 Cyp1b1*
Regulation Of Angiogenesis (GO:0045765)	2.38E-04	0.018548352 4946417	15.131266743207	126.22099785452	*Sparc Niban2 Nos3 Cyp1b1*
Nitric Oxide Metabolic Process (GO:0046209)	2.58E-04	0.018548352 4946417	101.8163265 30612	841.414238597364	*Nos3 Cyp1b1*
Regulation Of Biomineral Tissue Development (GO:0070167)	6.39E-04	0.038319697 6921103	61.9472049689441	455.6920507677	*Nos3 Sgms2*
Regulation Of Cell Population Proliferation (GO:0042127)	8.36E-04	0.042988318 8507511	6.319078947 36842	44.7834435401424	*Niban2 Nos3 Cyp1b1 Igfbp6 Nupr1 Pthlh*
Cellular Nitrogen Compound Biosynthetic Process (GO:0044271)	0.00104 905815 24956	0.047207616 8623022	47.4761904761904	325.680139401624	*Nos3 Cyp1b1*

Supplementary Table 3 (related to Extended Data Fig. 12c)

Term	*P* Value	Adjusted *P* Value	Odd Ratio	Combined Score	Genes
Extracellular Matrix Organization (GO:0030198)	5.84E-07	2.53E-04	7.753451677	111.2869272	*Col1a1 Postn Col3a1 Ccdc80 Col1a2 Flrt2 Col5a1 Col5a2 Mmp19 P3h4 Tgfbi*
Extracellular Structure Organization (GO:0043062)	6.24E-07	2.53E-04	10.37894737	148.2802045	*Col1a1 Postn Col3a1 Ccdc80 Col1a2 Col5a1 Col5a2 Mmp19 Tgfbi*
External Encapsulating Structure Organization (GO:0045229)	6.75E-07	2.53E-04	10.27566441	146.0066055	*Col1a1 Postn Col3a1 Ccdc80 Col1a2 Col5a1 Col5a2 Mmp19 Tgfbi*
Collagen Fibril Organization (GO:0030199)	1.96E-06	5.51E-04	18.95019157	249.0581039	*Col1a1 Col3a1 Col1a2 Col5a1 Col5a2 P3h4*
Skeletal System Development (GO:0001501)	8.39E-06	0.001886951	7.398496241	86.47365496	*Col1a1 Vkorc1 Bmp3 Pkdcc Col1a2 Zbtb16 Trps1 Pcsk5 Ets2*
Skin Development (GO:0043588)	3.37E-05	0.006311872	10.98887653	113.1657861	*Col1a1 Col3a1 Col1a2 Col5a1 Col5a2 Txnip*

Regulation Of Cell Migration (GO:0030334)	4.05E-05	0.006497672	3.895582329	39.40401069	*Ccl11* *Igfbp5* *Ldb1* *Mitf* *Sema3e* *Adarb1* *Podn* *Col1a1* *Bst2* *Gpnmb* *Ccl7* *Ctsh* *Spry2* *Amotl2*
Negative Regulation Of Cell Migration (GO:0030336)	1.17E-04	0.014820734	5.900975244	53.42883052	*Bst2* *Col3a1* *Igfbp5* *Hmox1* *Mitf* *Adarb1* *Trib1* *Podn*
Positive Regulation Of Canonical Wnt Signaling Pathway (GO:0090263)	1.19E-04	0.014820734	8.61676124	77.88821971	*Col1a1* *Sfrp4* *Lrrk1* *Nfkb1* *Dact1* *Rnf220*
Negative Regulation Of Cell Population Proliferation (GO:0008285)	1.72E-04	0.019388789	3.786103542	32.8070574	*Sfrp4* *Igfbp5* *Gpnmb* *Hmox1* *Nox4* *Ccn3* *Cxcl1* *Hes1* *Adarb1* *Trib1* *Podn* *B2m*
Regulation Of Non-Canonical Wnt Signaling Pathway (GO:2000050)	2.43E-04	0.024787148	30.52234206	254.0735832	*Sfrp4* *Rnf213* *Dact1*
Odontogenesis (GO:0042476)	4.08E-04	0.036934216	12.8474026	100.2624236	*Col1a1* *Osr2* *Col1a2* *Msx1*
Negative Regulation Of Mitotic Cell Cycle Phase Transition (GO:1901991)	4.50E-04	0.036934216	12.48989899	96.24392189	*Gpnmb* *Ccl2* *Zfp36l2* *Dact1*
Positive Regulation Of Wnt Signaling Pathway (GO:0030177)	4.60E-04	0.036934216	6.600937395	50.72297994	*Col1a1* *Sfrp4* *Lrrk1* *Nfkb1* *Rnf220* *Dact1*

Negative Regulation Of Nervous System Development (GO:0051961)	5.30E-04	0.037203116	22.37853107	168.8107272	*Ccl11* *Mbd1* *B2m*
Antigen Processing And Presentation Of Peptide Antigen Via MHC Class I (GO:0002474)	5.30E-04	0.037203116	22.37853107	168.8107272	*Tap2* *Ifi30* *B2m*

Supplementary Table 4 (related to Supplementary Fig. 15)

	p_val	avg_log2FC	pct.1	pct.2	p_val_adj	cluster	gene
1	1.39315939610369E-212	1.85432414836842	0.996	0.401	3.2768502155754 8E-208	Collecting	Vwf
2	2.06360532252468E-197	1.77675222777754	0.993	0.411	4.85380607911031 E-193	Collecting	Fabp4
3	1.95703782428205E-182	1.72775390180114	0.971	0.351	4.6031486664938 2E-178	Collecting	Cytl1
4	1.62675623733286E-180	1.97412301102022	0.969	0.364	3.8262933458306 2E-176	Collecting	Aqp1
5	4.16510422213897E-135	1.7016883236269	0.903	0.331	9.7967416408930 8E-131	Collecting	Rbp1
6	1.81337804577651E-109	3.09818164104902	0.621	0.111	4.2652465014709 3E-105	Collecting	Selp
7	4.16033755251543E-99	1.70694703044624	0.822	0.334	9.7855299572715 3E-95	Collecting	Clec14a
8	4.60733545060596E-95	2.04309474378339	0.727	0.226	1.0836913713370 3E-90	Collecting	Fabp5
9	1.39625575902279E-92	3.00658419367827	0.55	0.098	3.2841331707975 E-88	Collecting	Cygb
10	4.95680948917506E-86	1.83852969397189	0.721	0.244	1.16589115994887 E-81	Collecting	Ackr1
11	9.0994128981199E-76	1.77022809675745	0.653	0.203	2.1402729077667 8E-71	Collecting	Jam2
12	1.64619858095452E-66	2.13230139498924	0.541	0.144	3.8720236822631 4E-62	Collecting	Pltp
13	5.22371662277876E-63	2.56838318802802	0.489	0.118	1.2286703868437 9E-58	Collecting	Csf2rb
14	3.81527213413758E-62	1.7376558742612	0.518	0.134	8.9739015867050 1E-58	Collecting	Kcnc2
15	7.51147859727602E-61	1.70760290559228	0.575	0.181	1.7667748808652 9E-56	Collecting	Myrip
16	1.01095310226245E-66	1.63918465271277	0.957	0.684	2.3778627918315 E-62	Nos3_Collecting	Aopep
17	5.14888630861081E-59	1.91829517388589	0.838	0.392	1.21106954864835 E-54	Nos3_Collecting	Adipor2
18	1.28572246966416E-46	1.80604791023425	0.783	0.31	3.0241478208970 7E-42	Nos3_Collecting	Sparc
19	1.10629485739318E-43	1.77459679837916	0.834	0.458	2.60211613407449 E-39	Nos3_Collecting	Igfbp6
20	1.47325658577292E-43	1.87496268328894	0.762	0.34	3.4652468153964 8E-39	Nos3_Collecting	Fam20a
21	2.59864814201007E-43	2.72837752833511	0.396	0.048	6.11228029482189 E-39	Nos3_Collecting	Dcpp1
22	1.07791682506461E-41	1.391216246331	0.86	0.446	2.5353681642344 8E-37	Nos3_Collecting	Gria3
23	1.51594888140328E-39	1.77440914357719	0.791	0.471	3.5656633639486 6E-35	Nos3_Collecting	Klf3
24	5.58508939009232E-37	1.56383079916641	0.766	0.378	1.3136688754436 1E-32	Nos3_Collecting	Dcbld2
25	1.28273735627036E-36	1.51466825283371	0.749	0.308	3.0171265356835 1E-32	Nos3_Collecting	Sgms2
26	4.27642024272047E-33	1.39277220175763	0.83	0.519	1.0058568052902 8E-28	Nos3_Collecting	Nos3
27	1.71668952670597E-32	1.85461886657736	0.583	0.212	4.0378254357651 2E-28	Nos3_Collecting	Tead4
28	1.44164212567432E-30	2.05611520359548	0.54	0.183	3.3908864437985 6E-26	Nos3_Collecting	Gm14636

29	3.92536776465102E-30	1.84703627303965	0.587	0.238	9.2328575192356 6E-26	Nos3_Collecting	Fam135a
30	1.86025210944098E-27	2.48050180182575	0.46	0.152	4.3754989866161 2E-23	Nos3_Collecting	Cyp1b1
31	1.12325989032165E-75	2.26021957176329	0.908	0.302	2.6420195880255 5E-71	Foxp2_Collecting	Foxp2
32	1.24781366715748E-63	2.33758369291249	0.831	0.313	2.93498252652111 E-59	Foxp2_Collecting	Clca3a1
33	4.09791885335187E-62	1.97293079654304	0.892	0.285	9.6387149349689 3E-58	Foxp2_Collecting	Cldn5
34	1.82547869864424E-61	2.14152644407106	0.774	0.177	4.29370844708111 E-57	Foxp2_Collecting	Lcn2
35	7.78644309554199E-60	4.72611625768879	0.41	0.015	1.8314492805024 3E-55	Foxp2_Collecting	Ptprt
36	2.31877707197682E-57	3.77621359406518	0.497	0.046	5.4539955509966 8E-53	Foxp2_Collecting	Parm1
37	3.98767972660213E-55	2.97560554609606	0.626	0.111	9.3794214849408 8E-51	Foxp2_Collecting	Serpine2
38	8.21680130487431E-48	2.18863442136621	0.759	0.289	1.9326738349194 9E-43	Foxp2_Collecting	Glis3
39	9.12533932909559E-34	2.09546573712802	0.441	0.079	2.1463710635965 7E-29	Foxp2_Collecting	Kif26b
40	1.0389530355693E-30	2.88314755639605	0.328	0.038	2.4437214349625 5E-26	Foxp2_Collecting	Hs6st3
41	1.89772929626708E-30	1.75574230627646	0.641	0.291	4.4636490777497 9E-26	Foxp2_Collecting	Trf
42	1.91584918188317E-27	2.10128639023492	0.497	0.142	4.5062688607074 1E-23	Foxp2_Collecting	Marcksl1
43	2.42559658964273E-25	2.5622853756482	0.395	0.089	5.7052457384986 6E-21	Foxp2_Collecting	F2r
44	8.53638480762436E-25	1.83168512779921	0.544	0.18	2.0078430706013 3E-20	Foxp2_Collecting	Sema3d
45	2.21983355638065E-23	1.73092519435683	0.354	0.081	5.2212705079629 3E-19	Foxp2_Collecting	Btnl9
46	1.13053351468297E-257	9.10409666629349	0.976	0.016	2.6591278798858 E-253	Capillary	Ccl21a
47	2.20866095689043E-231	7.16564516924044	0.976	0.03	5.1949914367019 7E-227	Capillary	Reln
48	6.60512520335054E-226	7.0083905315875	0.937	0.057	1.5535914990800 8E-221	Capillary	Lyve1
49	5.31499622377448E-219	4.95970228301259	0.99	0.137	1.250140261794E-214	Capillary	Mmrn1
50	2.85860291487914E-161	7.70423954565971	0.768	0.008	6.7237199160872 2E-157	Capillary	Piezo2
51	1.03482525493405E-145	5.33128724749544	0.807	0.048	2.4340124821303 7E-141	Capillary	Pcsk6
52	1.46775352138242E-136	4.07531796360561	0.879	0.109	3.4523030576436 E-132	Capillary	Maf
53	3.08101630675987E-130	5.53120228325598	0.734	0.043	7.2468584551299 E-126	Capillary	Tgfbi
54	9.67843728392545E-113	4.60130902742758	0.725	0.057	2.2764652335521 E-108	Capillary	Col4a1
55	1.59038931944559E-101	5.82423148988195	0.609	0.026	3.7407547182679 6E-97	Capillary	Trps1
56	2.18445476004806E-99	9.06530785515027	0.493	0.001	5.13805604110904 E-95	Capillary	Apba2
57	5.72450350587388E-92	6.07796896729942	0.536	0.017	1.3464604696166 E-87	Capillary	Gmfg
58	6.00300966323583E-84	7.76416993701802	0.449	0.006	1.4119679028897 E-79	Capillary	Kcnn3
59	9.53895855054526E-83	4.11050391393132	0.623	0.072	2.2436584406737 5E-78	Capillary	Prelp

60	1.85740866811191E-79	4.19772857502104	0.594	0.078	4.3688109282660 3E-75	Capillary	Tspan18
61	5.00525643040273E-52	3.92985900508864	0.981	0.184	1.1772863649950 3E-47	Up Valve	Ednrb
62	1.04923988135337E-50	5.5473781778344	0.827	0.051	2.4679171249312 7E-46	Up Valve	Tmem108
63	4.86208606641202E-45	3.90442815458566	0.808	0.338	1.14361126368077 E-40	Up Valve	Slc41a1
64	4.83763760573024E-40	6.79323210131446	0.635	0.019	1.1378607412438 1E-35	Up Valve	Neo1
65	7.68170817790546E-35	3.51368090931925	0.827	0.188	1.8068145805251 4E-30	Up Valve	Ccdc141
66	5.18912522560699E-33	7.44805474224247	0.462	0.004	1.2205341443150 2E-28	Up Valve	Irx3
67	1.37191006447518E-32	3.12044454039863	0.942	0.208	3.2268696626520 6E-28	Up Valve	Nts
68	2.8648932353138E-32	4.27848741072194	0.692	0.055	6.7385153787815 9E-28	Up Valve	Lpl
69	1.29940023981782E-30	5.25620845951148	0.596	0.034	3.0563193040754 9E-26	Up Valve	Frmd5
70	4.97237227097306E-30	4.00072546820577	0.731	0.085	1.1695516818555 7E-25	Up Valve	Sox4
71	1.92707739994653E-29	3.1316646572938	0.827	0.179	4.5326787524142 4E-25	Up Valve	Ptn
72	2.14968024463597E-29	2.96076470154195	0.865	0.155	5.0562629034082 6E-25	Up Valve	Sema3a
73	2.46939420881466E-28	4.52422990501071	0.596	0.038	5.80826211855297 E-24	Up Valve	Tiam2
74	1.10138958507085E-27	7.10702603646258	0.385	0.003	2.5905784430451 4E-23	Up Valve	Pdcd1
75	2.07942949212382E-27	8.74741233517153	0.365	0.002	4.8910261084244 5E-23	Up Valve	Fxyd2
76	2.6660125348201E-119	9.20591317337374	0.691	0.006	6.2707280831503 6E-115	Down Valve	Coch
77	1.78021903567693E-116	6.2202424237599	0.77	0.041	4.1872531938157 E-112	Down Valve	Adm
78	5.43130104783539E-103	8.91789526572974	0.605	0.006	1.2774963194613 6E-98	Down Valve	Spp1
79	8.45931258889155E-83	6.04588571427739	0.605	0.021	1.9897149140331 8E-78	Down Valve	Hgf
80	2.48645435522457E-82	4.13360184095842	0.697	0.137	5.8483892889237 1E-78	Down Valve	Ltbp1
81	7.59758066596209E-80	3.17616037179637	0.868	0.202	1.7870269484409 4E-75	Down Valve	Prox1os
82	1.15782912373176E-72	4.39463751443745	0.664	0.173	2.7233298819294 8E-68	Down Valve	Angpt2
83	7.88943905361408E-71	5.10874100289262	0.572	0.033	1.8556749598005 7E-66	Down Valve	Fgf14
84	1.539585584469E-67	3.15623093713701	0.697	0.272	3.6212592532295 4E-63	Down Valve	Auts2
85	6.06353174414361E-67	4.19976348862181	0.612	0.065	1.4262033015400 2E-62	Down Valve	Cldn11
86	2.31204817025934E-62	5.74712140646824	0.474	0.021	5.438168501267E-58	Down Valve	Lypd6
87	1.68288859695588E-60	4.48770608076364	0.559	0.062	3.9583222688999 3E-56	Down Valve	Tmem45a
88	1.50110747180035E-59	3.44150484197024	0.684	0.159	3.5307548844216 1E-55	Down Valve	Nav2
89	9.87140243902854E-58	7.86379267774589	0.388	0.006	2.3218525676839 E-53	Down Valve	Dapl1
90	3.40617903626301E-49	3.34679110601403	0.572	0.09	8.01167371119423 E-45	Down Valve	Gm14964

Supplementary Table 5 (related to Supplementary Fig. 16)

	p_val	avg_log2FC	pct.1	pct.2	p_val_adj	cluster	gene
1	2.60207488063434E-160	5.62993370235853	0.882	0.047	6.12034032674003E-156	LSMC	Tesc
2	6.18823189742893E-160	5.11882176447822	0.912	0.097	1.45553402459426E-155	LSMC	Sorbs2
3	7.44665454626194E-151	3.72245665695176	0.951	0.275	1.75152761582627E-146	LSMC	Ptp4a3
4	5.42869823947009E-148	3.73780689558401	0.953	0.49	1.27688411290576E-143	LSMC	Crispld2
5	3.37826770007449E-129	4.39938277222397	0.872	0.113	7.94602345734521E-125	LSMC	Kcnab1
6	1.28556301344615E-125	10.5504150625189	0.707	0	3.02377276392669E-121	LSMC	Pln
7	2.56314706092756E-123	4.07870900208216	0.87	0.188	6.02877820200771E-119	LSMC	Vps37b
8	2.30746769116123E-86	4.02999240775717	0.701	0.092	5.42739475638033E-82	LSMC	Synm
9	1.55002531187461E-85	5.04837554338963	0.628	0.037	3.64581453606028E-81	LSMC	Map3k7cl
10	2.92313208183027E-80	3.7886886066971	0.703	0.118	6.87549896967297E-76	LSMC	Nrip2
11	1.94636536855764E-79	3.76970525408112	0.707	0.11	4.57804598338443E-75	LSMC	Cabp1
12	3.3145673210231E-75	4.62209044211163	0.607	0.047	7.79619379577843E-71	LSMC	Atp1a2
13	1.99378351521707E-71	9.20764631475554	0.466	0	4.68957820614207E-67	LSMC	Susd5
14	1.02096342776318E-66	3.89673792809252	0.583	0.058	2.40140807844176E-62	LSMC	Itpk1
15	1.18947968336274E-61	8.95141822680276	0.412	0	2.79777516323749E-57	LSMC	Fam81a
16	3.0196587987947E-106	5.50483325947055	0.927	0.079	7.10253946064501E-102	VSMC	Actg2
17	3.13691535985317E-81	3.74660379989789	0.92	0.205	7.37833861791065E-77	VSMC	Cnn1
18	7.2166211194425E-67	3.63530410562841	0.818	0.102	1.69742145350407E-62	VSMC	Sgcd
19	2.95383225735687E-66	3.61692188084402	0.818	0.105	6.9477088525291E-62	VSMC	Pcdh7
20	6.85919769632648E-62	5.18606893321755	0.65	0.039	1.61335189015295E-57	VSMC	Prlr
21	3.72654890790159E-61	3.97734838635206	0.73	0.073	8.76521568627533E-57	VSMC	Sytl2
22	1.82354581471968E-57	4.35625888142823	0.664	0.055	4.28916211080216E-53	VSMC	Crlf1
23	1.74562688525881E-54	7.7463510818738	0.482	0.006	4.10588899681724E-50	VSMC	Cpa6
24	4.40386062532409E-53	4.30493061727733	0.628	0.058	1.03583205768248E-48	VSMC	Npnt
25	1.81818773097409E-49	7.666244410338	0.438	0.004	4.27655936202417E-45	VSMC	Fam227b
26	6.47058628146149E-46	4.29655375060609	0.555	0.042	1.52194659926256E-41	VSMC	Frmpd4
27	9.47746506992914E-46	6.46426088017154	0.438	0.01	2.22919455909803E-41	VSMC	Lhx8
28	1.48754818006242E-43	8.00442980390666	0.401	0.006	3.49886207432482E-39	VSMC	Grem1
29	7.9332797272222E-42	3.87572586431918	0.555	0.053	1.86598672463993E-37	VSMC	Rerg

30	1.38919482547154E-41	3.93298218571704	0.54	0.046	3.26752514899161E-37	VSMC	Rasgrf1
31	2.02414600994581E-178	6.10403931054725	0.97	0.429	4.76099382999354E-174	Dcnhigh_Pericyte	Dcn
32	1.36565992277377E-106	5.1111851237546	1	0.304	3.21216870435618E-102	Dcnhigh_Pericyte	Apoe
33	5.27204245510241E-64	5.62419999906122	0.713	0.079	1.24003710586464E-59	Dcnhigh_Pericyte	Dpt
34	3.07101062853958E-43	4.04854282559099	0.673	0.079	7.22332409938794E-39	Dcnhigh_Pericyte	Plxdc2
35	1.24823667128255E-42	5.26530497757251	0.554	0.031	2.93597747452369E-38	Dcnhigh_Pericyte	Fmo2
36	2.67655202524138E-41	6.26852883578399	0.495	0.029	6.29551801857026E-37	Dcnhigh_Pericyte	Lum
37	1.902214818999E-39	4.20524875523956	0.614	0.1	4.47419947576754E-35	Dcnhigh_Pericyte	Ctsc
38	3.98420809374058E-37	5.02847332289419	0.554	0.053	9.37125585728721E-33	Dcnhigh_Pericyte	Igf1
39	1.4898372024019E-36	9.21395250035212	0.366	0.001	3.50424608376951E-32	Dcnhigh_Pericyte	Cacna1e
40	2.65100026171116E-36	6.0730018370604	0.436	0.019	6.23541771557082E-32	Dcnhigh_Pericyte	Sfrp4
41	3.6235409412356E-32	5.38054896687504	0.446	0.069	8.52293064788024E-28	Dcnhigh_Pericyte	Has1
42	2.72558887865419E-31	9.37990277773548	0.327	0.003	6.41085760148252E-27	Dcnhigh_Pericyte	Gsta3
43	6.22901983237934E-30	4.88194385714645	0.436	0.041	1.46512775477394E-25	Dcnhigh_Pericyte	Col14a1
44	1.4049566945437E-29	4.89140603552353	0.475	0.055	3.30459864123623E-25	Dcnhigh_Pericyte	Penk
45	4.24680471234072E-29	4.5414725870011	0.406	0.02	9.9889093638966E-25	Dcnhigh_Pericyte	Ptgs2
46	3.34771674392122E-96	3.84109124327403	0.965	0.142	7.87416455337711E-92	Dcnlow_Pericyte	Steap4
47	2.35900821362048E-92	4.77230787786725	0.833	0.133	5.54862321925673E-88	Dcnlow_Pericyte	Kcnq5
48	2.22140017116691E-74	5.82468384588221	0.688	0.031	5.22495534260169E-70	Dcnlow_Pericyte	Cyp4b1
49	6.02388124937561E-70	3.30236094304011	0.854	0.225	1.41687710866564E-65	Dcnlow_Pericyte	Septin4
50	1.83942317975314E-65	3.86603126005637	0.792	0.136	4.32650726109737E-61	Dcnlow_Pericyte	Adamts12
51	2.16846305641529E-56	4.78800330391392	0.604	0.038	5.1004419549944E-52	Dcnlow_Pericyte	Dlk1
52	3.75834914385926E-52	3.48401744085612	0.743	0.136	8.84001302127136E-48	Dcnlow_Pericyte	Rgs16
53	3.62764373521739E-51	6.72136672360797	0.493	0.02	8.53258082960483E-47	Dcnlow_Pericyte	Ednrb
54	4.87183451706633E-49	4.32599590680989	0.549	0.034	1.14590419675917E-44	Dcnlow_Pericyte	Tnfrsf21
55	4.924674772628E-45	5.23709312297858	0.465	0.018	1.15833275326983E-40	Dcnlow_Pericyte	Adgrf5
56	1.52459524457385E-43	3.13554396763811	0.653	0.102	3.58600047476216E-39	Dcnlow_Pericyte	Agmo
57	2.82806139133849E-43	4.29506966950571	0.535	0.052	6.65188319856726E-39	Dcnlow_Pericyte	Cd36
58	9.07640931468732E-43	3.12101996771702	0.785	0.241	2.1348622349076E-38	Dcnlow_Pericyte	Fabp4
59	2.23434348372663E-41	4.5014517994357	0.521	0.052	5.2553993080734E-37	Dcnlow_Pericyte	Mndal
60	6.00198271828639E-40	3.32968932274317	0.611	0.101	1.41172635516814E-35	Dcnlow_Pericyte	Ly6e

Supplementary Table 6 (related to Supplementary Fig. 17)

	p_val	avg_log2FC	pct.1	pct.2	p_val_adj	cluster	gene
1	0	2.19276744460826	0.922	0.299	0	Dpp4_Fibroblast	Dpp4
2	0	1.88611328187278	0.86	0.277	0	Dpp4_Fibroblast	Pcsk6
3	0	2.00764355942699	0.943	0.368	0	Dpp4_Fibroblast	Anxa3
4	0	2.50753284311742	0.803	0.259	0	Dpp4_Fibroblast	Smpd3
5	0	2.12008926041189	0.783	0.251	0	Dpp4_Fibroblast	Efhd1
6	0	1.96923594736457	0.722	0.218	0	Dpp4_Fibroblast	Tek
7	0	1.85424554607043	0.676	0.209	0	Dpp4_Fibroblast	Pla1a
8	0	2.07279347200687	0.924	0.464	0	Dpp4_Fibroblast	Sema3c
9	0	2.69392557442205	0.534	0.125	0	Dpp4_Fibroblast	Duoxa1
10	0	2.0821592648565	0.615	0.213	0	Dpp4_Fibroblast	Ston2
11	0	1.85944705767977	0.983	0.607	0	Dpp4_Fibroblast	Fndc1
12	0	1.82541323382251	0.566	0.211	0	Dpp4_Fibroblast	Cmah
13	0	2.67497998410477	0.457	0.111	0	Dpp4_Fibroblast	Aif1l
14	0	1.95858672999385	0.514	0.168	0	Dpp4_Fibroblast	Eya4
15	0	2.86251121778668	0.444	0.104	0	Dpp4_Fibroblast	Ccn3
16	0	2.60212742478086	0.903	0.315	0	Postn_Fibroblast	Gm56555
17	0	3.14582702970428	0.722	0.206	0	Postn_Fibroblast	Gm56730
18	0	2.10116251171294	0.824	0.339	0	Postn_Fibroblast	Pde10a
19	0	2.46645908613292	0.955	0.479	0	Postn_Fibroblast	Gm20186
20	0	2.02211462519865	0.858	0.41	0	Postn_Fibroblast	Kdm7a
21	0	1.9546264242171	0.932	0.549	0	Postn_Fibroblast	Zbtb16
22	0	2.11688786643619	0.952	0.614	0	Postn_Fibroblast	Aig1
23	0	1.72318586854195	0.956	0.713	0	Postn_Fibroblast	Eif4e
24	2.20383E-319	2.05363507267743	0.807	0.371	5.18362671E-315	Postn_Fibroblast	Gm56906
25	1.32886160843E-313	1.81937407425706	0.878	0.522	3.125615389190042E-309	Postn_Fibroblast	Jarid2
26	3.43673759703587E-296	1.65874521014811	0.897	0.456	8.083550501988808E-292	Postn_Fibroblast	Ptprj
27	6.53624624211829E-279	2.34843306397339	0.649	0.191	1.537390478608864E-274	Postn_Fibroblast	Uty
28	9.31644257003847E-254	1.78867839791376	0.773	0.362	2.191320456898875E-249	Postn_Fibroblast	Adarb1
29	1.45032971190334E-234	2.27576595071361	0.633	0.211	3.411320515367685E-230	Postn_Fibroblast	Rian
30	4.34819551296566E-209	1.72860291663423	0.715	0.309	1.022739066604650E-204	Postn_Fibroblast	Gramd3
31	0	2.85376641283178	0.878	0.316	0	Cxcl14_Fibroblast	Gas6
32	0	2.72501374566195	0.717	0.178	0	Cxcl14_Fibroblast	Steap4
33	0	4.18730614238584	0.599	0.08	0	Cxcl14_Fibroblast	Cxcl14
34	0	2.53296007236912	0.89	0.371	0	Cxcl14_Fibroblast	Gdf10
35	0	3.26740579918596	0.604	0.117	0	Cxcl14_Fibroblast	Tmem176b
36	0	3.12588810207517	0.524	0.072	0	Cxcl14_Fibroblast	Col15a1
37	0	2.37131776346613	0.636	0.184	0	Cxcl14_Fibroblast	Sparcl1
38	0	2.38597447373649	0.564	0.142	0	Cxcl14_Fibroblast	Tspan11
39	0	3.25311657328401	0.508	0.089	0	Cxcl14_Fibroblast	Tmem176a
40	0	2.3842721843729	0.56	0.156	0	Cxcl14_Fibroblast	Clec11a
41	0	2.70366843662899	0.663	0.273	0	Cxcl14_Fibroblast	Penk
42	0	2.32840219541272	0.557	0.181	0	Cxcl14_Fibroblast	Spon1
43	0	2.08112636736414	0.988	0.615	0	Cxcl14_Fibroblast	Igfbp7
44	0	2.68505666938615	0.821	0.459	0	Cxcl14_Fibroblast	Apoe
45	0	2.15340623878751	0.705	0.357	0	Cxcl14_Fibroblast	Mmp3
46	3.37119631903098E-146	4.79156611634826	0.7	0.07	7.929390861992276E-142	Ptgfr_Fibroblast	Ptgfr
47	1.97315538812825E-142	7.6166021964186	0.556	0.008	4.641058788416646E-138	Ptgfr_Fibroblast	Lgr5

48	1.261103459 68978E-136	3.14209722775977	0.931	0.431	2.9662414475 3632E-132	Ptgfr_Fibroblast	Itm2a
49	9.658721327 38244E-130	5.34432771948774	0.669	0.033	2.2718278434 1362E-125	Ptgfr_Fibroblast	Stk32a
50	1.117730305 88085E-127	3.18673027428649	0.9	0.553	2.6290134524 6236E-123	Ptgfr_Fibroblast	Eln
51	7.653858866 64333E-123	3.92597223427101	0.863	0.12	1.8002641440 2318E-118	Ptgfr_Fibroblast	Mfap4
52	7.848724933 05851E-115	4.08503890736789	0.681	0.104	1.8460985915 0469E-110	Ptgfr_Fibroblast	Col4a5
53	2.149556796 17871E-108	3.42857350653256	0.819	0.218	5.0559725402 9194E-104	Ptgfr_Fibroblast	Crispld2
54	6.700096377 95613E-101	3.84308985735154	0.637	0.122	1.5759296690 5906E-96	Ptgfr_Fibroblast	Tgm2
55	9.983740678 54068E-96	4.00920340288899	0.706	0.082	2.3482756449 9955E-91	Ptgfr_Fibroblast	Pakap.1
56	1.500723567 65781E-89	7.33636977632882	0.362	0.005	3.5298519034 8794E-85	Ptgfr_Fibroblast	Dach1
57	1.324353671 3296E-81	3.75675158749684	0.506	0.131	3.1150122703 3435E-77	Ptgfr_Fibroblast	Aldh1a1
58	1.777929804 4582E-77	3.16733494728729	0.744	0.125	4.1818686930 6613E-73	Ptgfr_Fibroblast	Cpe
59	1.968985881 76863E-76	4.53200128925528	0.475	0.022	4.6312516925 08E-72	Ptgfr_Fibroblast	Cacna1g
60	3.396894286 76838E-76	3.39374240211163	0.662	0.103	7.9898350519 079E-72	Ptgfr_Fibroblast	Gnai1
61	0	4.60123345157466	0.851	0.127	0	Fmod_Fibroblast	Ccdc3
62	0	4.54572995755349	0.812	0.105	0	Fmod_Fibroblast	Fxyd6
63	0	4.8817825473386	0.688	0.049	0	Fmod_Fibroblast	Arhgdib
64	0	5.0240858268963	0.702	0.086	0	Fmod_Fibroblast	Fhl2
65	0	5.408210397255	0.628	0.051	0	Fmod_Fibroblast	Ccn2
66	0	7.93453179054364	0.56	0.004	0	Fmod_Fibroblast	Fmod
67	0	7.13660452397087	0.548	0.011	0	Fmod_Fibroblast	Colec11
68	0	7.28027166461418	0.512	0.006	0	Fmod_Fibroblast	Acsbg1
69	6.248905516 66143E-303	4.5022412748372	0.63	0.065	1.4698050665 7393E-298	Fmod_Fibroblast	Cpxm2
70	7.256019861 3215E-294	6.12041410453173	0.479	0.014	1.7066884315 8143E-289	Fmod_Fibroblast	Foxd1
71	4.268181243 85263E-291	5.67015899098408	0.506	0.016	1.0039189103 6658E-286	Fmod_Fibroblast	Egflam
72	6.533916280 90445E-288	6.77610679322333	0.44	0.008	1.5368424484 3154E-283	Fmod_Fibroblast	Nkain4
73	1.654711600 24974E-257	6.29919070956801	0.417	0.01	3.8920471549 4741E-253	Fmod_Fibroblast	Ptprb
74	8.014273204 12228E-250	6.56862198923322	0.39	0.006	1.8850372003 416E-245	Fmod_Fibroblast	Nog
75	1.836631995 55442E-243	4.63042986623397	0.508	0.043	4.3199421167 4354E-239	Fmod_Fibroblast	Gfra2